BRITISH GEOLOGICAL SURVEY

Natural Environment Research Council

TECHNICAL REPORT WD/99/18 Hydrogeology Series

Technical Report WD/99/18

Modelling the Development of Fracture Aperture Distributions using a Simple Aperture Growth Law

John P Bloomfield and John A Barker¹

¹ University College London

Bibliographic Reference

Bloomfield J P and Barker, J A 1999
Modelling the Development of
Fracture Aperture Distributions
using a Simple Aperture Growth Law
British Geological Survey Report WD/99/18



BRITISH GEOLOGICAL SURVEY

BRITISH GEOLOGICAL SURVEY KEYWORTH NOTTINGHAM NG12 5GG UNITED KINGDOM

TEL (0115) 9363100 FAX (0115) 9363200

DOCUMENT TITLE AND AUTHOR LIST

Modelling the Development of Fracture Aperture Distributions using a Simple Aperture Growth Law John P Bloomfield and John A Barker

CLIENT	CLIENT REPORT #		
	BGS REPORT#	WD/99/18	
	CLIENT CONTRACT REF		
	BGS PROJECT CODE	76CMD12	
	CLASSIFICATION	Open	

	SIGNATURE	DATE		SIGNATURE	DATE
PREPARED BY (Lead Author)	FPBoomfield	30,499	CO-AUTHOR		
			CO-AUTHOR		
PEER REVIEWED BY	-0.77	12/01/64	CO-AUTHOR		
	TRISh	18/06/11	CO-AUTHOR		
CHECKED BY	11,100	7 1 /04	CO-AUTHOR		
(Project Manager or deputy)	Lon Delo	2 July 17	CO-AUTHOR		
APPROVED BY			CO-AUTHOR		
(Project Director or senior staff)			CO-AUTHOR		
APPROVED BY (Hydrogeology Group Manager)		2/7/99	OS Copyright acknowledged		
Layout checked by	C. Sharatt	2/7/99	Assistant Director clearance (if reqd)		

BRITISH GEOLOGICAL SURVEY

The full range of Survey publications is available from the BGS Sales Desk at the Survey headquarters, Keyworth, Nottingham. The more popular maps and books may be purchased from BGS-approved stockists and agents and over the counter at the Bookshop, Gallery 37, Natural History Museum, Cromwell Road, (Earth Galleries), London, Sales Desks are also located at the BGS London Information Office, and at Murchison Edinburgh. The London House. Information Office maintains a reference collection of BGS publications including maps for consultation. Some BGS books and reports may also be obtained from HMSO Publications Centre or from HMSO bookshops and agents.

The Survey publishes an annual catalogue of maps, which lists published material and contains index maps for several of the BGS series.

The British Geological Survey carries out the geological survey of Great Britain and Northern Ireland (the latter as an agency service for the government of Northern Ireland), and of the surrounding continental shelf, as well as its basic research projects. It also undertakes programmes of British technical aid in geology in developing countries as arranged by the Department for International Development.

The British Geological Survey is a component body of the Natural Environment Research Council. Keyworth, Nottingham NG12 5GG

~ 0115-936 3100

Telex 378173 BGSKEY G Fax 0115-936 3200

Murchison House, West Mains Road, Edinburgh, EH9 3LA

***** 0131-667 1000

Telex 727343 SEISED G

Fax 0131-668 2683

London Information Office at the Natural History Museum, Earth Galleries, Exhibition Road, South Kensington, London SW7 2DE

2 0171-589 4090

Fax 0171-584 8270

☎ 0171-938 9056/57

St Just, 30 Pennsylvania Road, Exeter EX4 6BX

***** 01392-78312 Fax 01392-437505

Geological Survey of Northern Ireland, 20 College Gardens, Belfast BT9 6BS

3 01232-666595

Fax 01232-662835

Maclean Building, Crowmarsh Gifford, Wallingford, Oxfordshire OX10 8BB

☎ 01491-838800

Fax 01491-692345

Parent Body
Natural Environment Research Council
Polaris House, North Star Avenue, Swindon, Wiltshire
SN2 1EU

***** 01793-411500

Telex 444293 ENVRE G Fax 01793-411501

Contents

ACKNOWLEDGEMENTS

ABSTRACT

1.	HYD	ROGEOLOGICAL CONTEXT	1
2.	PREV	VIOUS STUDIES AND RATIONALE OF THE PRESENT STUDY	3
	2.1	Previous Studies	3
	2.2	Rationale of the Present Study	4
3.	THE	MODEL	6
	3.1	Mathematical Description of the Model	6
	3.2	Numerical Implementation within the EVOLVER Code	8
	3.3	Range of Investigation	9
4.	RESU	JLTS	12
	4.1	Evolution in Transmissivity as a Function of Aperture Growth-rate	16
5.	DISC	CUSSION	17
	5.1	Structural Evolution in the Fracture Aperture Arrays	17
	5.2	Geometrical Phase Transitions in the Evolved Aperture Arrays	19
	5.3	Transmissivity of the Evolved Aperture Arrays	23
	5.4	Limitations of the Model	27
	5.5	Requirements for a Quantitative Description of Dynamic Systems such as	20
		EVOLVER	28
6.	SUM	MARY	30
7.	FUT	URE WORK	31
	7.1	Review	31
	7.2	Theoretical Development	31
	7.3	Code Development	32
	7.4	Model Validation	33
	7.5	Scaling Phenomena in Simple Systems	33
	7.6	Case Studies	33
REF	ERENCI	ES	35
NOT	ATION		40

List of Figures

- Figure 1. Boundary conditions for the EVOLVER model.
- Figure 2. Maps showing the effect of variations in the aperture growth-rate exponent on the form of evolved aperture arrays. Runs 35, 29, 30, 27, 32 and 34 correspond to aperture growth-rate exponents 0.2, 0.3, 0.4, 0.5, 0.6 and 0.7 respectively. Each map is based on an initial aperture distribution with a mean of $\log_{10} 0$ and σ_{a0} of $\log_{10} 0.3$, where all the maps show the evolved structure at time 100.
- Figure 3. Lognormal probability plots of aperture data for maps generated with aperture growth-rate exponents 0.2, 0.4, 0.6 and 0.8 (runs 50, 30, 32 and 33 respectively). All runs were performed on an initial aperture distribution with a mean of $\log_{10} 0$ and σ_{a0} of $\log_{10} 0.3$. Five aperture populations are shown in each probability plot, corresponding to the initial aperture distribution and distributions at times 100, 200, 300 and 600.
- Figure 4. Illustration of the development of aperture sub-populations given an aperture growthrate exponent of 0.6 ($\sigma_{a0} = \log_{10} 0.3$ and t = 100). The lognormal probability plot shows three approximately lognormal aperture sub-populations.
- Figure 5. Illustration of the effect of σ_{a0} on the geometry of the single array-spanning path. The fracture aperture maps (t = 100) were all generated using an aperture growth-rate exponent of 0.7. Runs 43, 44, 34, 45, 41 and 46 correspond to $\sigma_{a0} = \log_{10} 0.1$, 0.2, 0.3, 0.4, 0.5 and 0.6 respectively. The tortuosity of the preferentially enlarged array spanning paths increases up to a maximum of about three for $\sigma_{a0} = \log_{10} 0.5$
- Figure 6. Variation in tortuosity as a function of σ_{a0} .
- Figure 7. Variation in effective transmissivity of six fracture arrays with aperture growth-rate exponents in the range 0.2 to 0.7 up to time 100 ($\sigma_{a0} = \log_{10} 0.3$ and $a_0 = \log_{10} 0$).
- Figure 8. Nine aperture maps illustrating the development of geometrically stable structures at early times in the evolution of the arrays. The maps on the left-hand side of the figure are full maps for arrays at times 0, 10 and 40. The centre and right-hand maps are plots of the largest 25 and 10% of fractures at each of the three time steps.
- Figure 9. Examples of changes in flow rate with time in selected fractures during the early stages of growth of an array where an array-spanning structure develops.
- Figure 10. Plot of σ_{row} against aperture growth-rate exponent and time (up to 1000) for the six runs shown in Figure 2, and for run 33 shown in Figure 3. The data have been contoured to emphasise the trends in the surface. Three geometrical regimes are indicated.
- Figure 11. Three aperture maps illustrating the effect of a_0 on the form of evolved aperture arrays. All fracture maps were generated using an aperture growth rate exponent of 0.6 and using $\sigma_{a0} = \log_{10} 0.3$. Figure 11a was generated using an initial mean aperture of $\log_{10} 1$, and Figures 11b and 11c using initial mean apertures of 0 and -1 (runs 48, 37 and 47 respectively). Lower initial mean apertures lead to the promotion of single array-spanning paths at constant σ_{a0} , and higher initial mean apertures lead to more heterogeneous, but relatively isotropic, structures.

- Figure 12. Illustration of the uncertainties in characterising the form of aperture arrays near a phase change boundary. The plot shows how σ_{row} varies with time for an aperture growth-rate exponent of 0.6 and σ_{a0} of \log_{10} 0.3. The solid circles are mean values based on fourteen independent realisations (error bars 1 S.D.). Runs with the maximum and minimum evolved values of σ_{row} are also shown, as are their corresponding aperture maps.
- Figure 13. Variation in $T_{crit(map)}/T_{eff}$ as a function of time for aperture growth-rate exponents in the range 0.2 to 0.7 ($\sigma_{a0} = \log_{10} 0.3$ and $a_0 = \log_{10} 0$). Error bars on the 0.7, 0.5 and 0.3 aperture growth-rate exponent curves are based on ten runs at each condition (see Figure 7 for key).
- Figure 14. Illustration of the effects of relaxing the 'cubic law' condition. The figure shows three evolved aperture arrays at time 100 ($\sigma_{a0} = \log_{10} 0.3$, $a_0 = \log_{10} 0$ and e = 0.6), where Figures 14a, 14b and 14c were generated with g = 2, 2.5 and 3 respectively. Figure 14d shows T_{eff} as a function of time for five values of g between 2 and 3.

List of Tables

Table 1. Values of T_{crit} and T_{eff} for the initial aperture distributions of six runs ($\sigma_{a0} = \log_{10} 0.3$ and $a_0 = \log_{10} 0$). Values of $T_{crit(map)}$ were found using the map construction method and values of $T_{crit(50th)}$ were calculated from the 50th percentile of the ranked aperture distribution.

ACKNOWLEDGEMENTS

We would like to thank Ruaraidh Mackenzie (University College London) for computational support and Nicky Robinson (University College London), Ann Williams and Bob Shearer for their helpful review comments. Some of the work described in the paper was undertaken as part of the National Groundwater Survey (JPB), and is published by permission of the Director of the British Geological Survey.

ABSTRACT

Fractures in shallow sedimentary aquifers may become enlarged over relatively short geological time scales due to groundwater circulation. The aim of the present study is to develop a model to investigate general relationships between fracture aperture growth and the geometry of evolved fracture arrays using a simple aperture growth law and simple aperture geometries. The evolution in the conductivity of the system is also investigated. The model is formulated as an initial value problem and it has been used to study the growth of an array of orthogonal fractures with an initial, spatially uncorrelated, lognormal aperture distribution, where aperture growth-rate is an exponent of the flow rate through each fracture. The geometries of the evolved aperture arrays display a range of self-organised structures that are sensitive to the aperture growth-rate exponent, e, and to the standard deviation of the initial aperture distribution, σ_{a0} . They show geometrical phase changes in the evolved structure as a function of changes in the boundary conditions. For example, low values of e and σ_{a0} lead to bi-modal aperture distributions, where apertures perpendicular to flow undergo limited growth and apertures parallel to flow are preferentially enlarged. At moderate values of e and σ_{a0} , there is a transition to a regime of more complex aperture geometries with anastomosing, channel-like, structures of preferentially enlarged apertures. At larger values of e, single continuous channel-like paths of preferentially enlarged apertures develop, where the tortuosity of the channel-like paths is a As they develop, the arrays show a power-law like increase in effective function of σ_{a0} . transmissivity, with transmissivity inversely proportional to e. Continuum percolation models provide a good description of the conductivity of the initial aperture arrays. However, because of selforganisation in the evolved aperture arrays, the conductivity of most of the evolved networks departs systematically from that predicted by continuum percolation theory. Future work is to be funded by the NERC Micro-to-Macro Thematic Programme. It will involve the development of a theoretical framework to describe the dynamic behaviour of evolving porous media, code development, model validation, investigation of scaling and self-organisation phenomena in simple systems, and case studies including the investigation of enlarged fractures in the Chalk.

1. HYDROGEOLOGICAL CONTEXT

A characteristic feature of many fractured sedimentary aquifers is their hydraulic heterogeneity. Hydraulic conductivity may vary by many orders of magnitude over relatively small distances and may vary significantly with depth. In addition, rapid flow paths, as identified by tracer tests, can be highly localised. It is thought that the hydraulic variability of fractured sedimentary aquifers is primarily due to preferential channelling of flow through components of the fracture network over a range of scales. The hydraulic heterogeneity of such aquifers has important implications for the effective management of water supplies and particularly for the delineation of defensible source protection zones around public supply boreholes. It is important therefore to develop predictive models that reduce the uncertainty associated with characterising these aquifers, and there is a specific need to include preferential flow paths in a realistic manner in models of these systems.

Because our knowledge of fractured rock is intrinsically uncertain, probabilistic computational methods are almost invariably used to generate 'realistic' single fractures or fracture networks. Modelling studies have investigated relationships between fracture characteristics and flow and transport phenomena in single fractures [Tsang, 1984; Smith and Schwartz, 1984; Moreno et al., 1988; Tsang et al., 1988; Tsang and Tsang, 1987, 1989] and in fracture networks [Andersson and Dverstrop, 1987; Cacas et al., 1990a, b; Dverstorp et al., 1992; Nordqvist et al., 1992; David, 1993; Tsang, 1993; Nordqvist et al., 1998] using stochastic descriptions of the fractures. Many of these studies have concentrated on predicting contaminant breakthrough curves. These studies have shown that flow and transport in fracture arrays are affected by the breadth of the fracture aperture distribution, and features of the fracture network architecture, such as the nature of fracture connectivity. Margolin et al. [1998] demonstrated how both fracture geometry and fracture aperture variability could lead to channelled flow. They developed a functional relationship that quantified the dependence of effective hydraulic conductivity on aperture variability, network structure, and fracture element density. Percolation theory has also been used to describe flow and transport in fracture networks [Berkowitz and Balberg, 1993; Berkowitz, 1995]. Fracture networks with a broad distribution of aperture sizes near the percolation threshold exhibit critical path geometries and transport properties that may be characterised by power law relationships.

To date, studies of channelling of flow in fracture networks have generally assumed that the geometries of fracture networks and the fracture aperture distributions are independent of flow through the network, for example *David* [1993] (studies of karst development are an exception, see section 2). This is because flow channelling is more easily modelled in relatively simple systems that do not undergo structural development, and because many of the studies have been related to investigations of deep waste disposal sites in fractured hard rocks. In hard rocks, fracture network characteristics may be modified by processes such as sub-critical crack growth [*Dienes*, 1982; *Atkinson*, 1984; *Gueguen et al.* 1986; *Renshaw*, 1996] and the elastic opening of fractures due to changes in overburden [*Tsang and Witherspoon*, 1981; *Walsh*, 1981; *Brown and Scholz*, 1985a]. Although these processes are sensitive to pore fluid pressure they will not be affected by groundwater flow. Mineralization of components of the fracture network may reduce the total fracture porosity, however, even over the relatively long time-scales typical of safety cases for radioactive waste repositories, enlargement of fracture apertures due solely to groundwater circulation may be negligible in most hard rocks.

In contrast, fracture network geometries, and specifically fracture aperture distributions, in sedimentary aquifers, particularly poorly consolidated fractured sandy aquifers or fractured carbonate aquifers, such as the Chalk aquifer of north west Europe, may be modified significantly over relatively short geological time-scales. Three principal classes of process are thought to be involved in the development of enlarged fracture porosity due to groundwater flow. These are dissolution, plucking and mechanical wear. Each of these classes of fracture enlargement may be expected to exhibit characteristic constitutive relationships between rate of fracture growth and groundwater flow velocity in the fracture. It is reasonable to assume that in nature these processes will probably not operate in isolation. In addition, each of the fracture

enlargement processes will be affected significantly by both the chemical environment and, particularly in shallow aquifers, by microbiological activity.

In sedimentary aquifers that are prone to enlargement of the fracture network by groundwater flow, the development of flow channelling will not simply be a geometrical artefact of aperture variability, network structure, and fracture element density (as described by *Margolin et al.* [1998]). Channelling of flow will be affected by the nature of the feedback processes between groundwater flow and rock structure. Natural systems that develop through feedback characteristically display a range of self-organised or emergent structures whose geometry depends on the nature of the feedback process [e.g. *Bak et al.* 1988; *Bak* 1996; *Holland* 1998]. The term emergence is used to describe the phenomena of persistent or recurring structures arising as the product of coupled, non-linear, context-dependent interactions, where the overall behaviour of the system cannot be obtained by summing the behaviour of its constituent parts [*Holland* 1998]. Features of systems that exhibit emergence include:

- multiple, interacting copies of a feature with common properties (e.g. fracture size and aperture)
- the configuration of the interacting elements can change with time (e.g. hydraulic head and flow distributions, and fracture apertures may change with time), and
- interactions between the system elements are constrained by 'rules', usually non-linear (e.g. rules governing fracture aperture growth, either process dependent constitutive relationships or effective growth laws, and rules relating hydraulic head and flow through fracture arrays).

From the above it is clear that where fracture networks undergo enlargement due to groundwater flow the resulting structures and flow geometries may be considered as emergent features of the system.

The aim of the present study is to develop a model to investigate general relationships between fracture aperture growth and the geometry of evolved fracture apertures using generic growth laws and simple fracture geometries. We see this modelling as a step up in complexity from investigating channelling in fracture networks that do not develop due to flow. The work is intended as a precursor to future systematic studies of the emergent behaviour of dynamic fractured aquifer systems, of modelling natural fracture geometries, and effective aperture growth laws. Consequently, an additional aim is to identify requirements for the future quantitative description of dynamic systems.

2. PREVIOUS STUDIES AND RATIONALE OF THE PRESENT STUDY

2.1 Previous Studies

There have been many geochemical modelling studies of solution, transportation, and precipitation of reactive solutes in fractures and fracture networks (usually in carbonate systems) and a concise review can be found in *Dijk and Berkowitz* [1998]. A common approach is to specify a mass balance where the rate of fracture enlargement is taken to be proportional to the product of the flux in the fracture and the (carbonate) dissolution rate, where the flux in the fracture is assumed to be proportional to the fracture aperture. The rate of dissolution is proportional to a reaction rate co-efficient, solute concentration in the flowing fracture, and to the fracture geometry. *Dijk and Berkowitz* [1998] showed that in such systems the evolution of the solute transport and fracture geometry can be described adequately using the Damkohler and Peclet numbers.

There have been numerous studies specifically investigating the formation and development of karst in carbonates rocks [e.g. *Palmer*, 1975, 1991; *White*, 1977; *Dreybrodt*, 1990; *Groves and Howard*, 1994a, 1994b; *Howard and Groves*, 1995; *Dreybrodt*, 1996; *Siemers and Dreybrodt*, 1998]. The primary aims of these studies have been to understand the processes of karst formation and development, and to produce models capable of replicating the range of observed karst system geometries.

Assuming laminar flow, Weyl [1958] calculated a karstic 'penetration length', the length that water can flow through natural fractures before it becomes fully saturated. This was found to be of the order of millimetres to metres: a significantly shorter length than that of typical karstic features. White [1977] showed that calcite dissolution rates fall rapidly as water in fractures nears saturation and that although the rate of dissolution may be relatively slow down gradient, unsaturated water may extend through the fracture system over much greater lengths than predicted by Weyl [1958]. If the down gradient sections of the fracture system can be enlarged at even relatively slow rates, then flow velocities within the system increase with time and relatively unsaturated water will reach further into the fracture network [Dreybrodt, 1990; Groves and Howard, 1994a].

Groves and Howard [1994a] defined three rate-limiting kinetic mechanisms to the growth of karstic conduits: the rate of reaction at rock-water interfaces, the rate of diffusion of calcium ions from rock surfaces to the bulk solution, and the rate of CO₂ hydration of the bulk solution. They developed a model that identified the limiting step for any set of chemical or flow conditions, and used this, to asses the minimum hydrochemical conditions that allowed karstic development, and to predict to form of karstic systems that would develop. Given geologically reasonable conditions, and assuming laminar flow, they found that minimum initial fracture apertures of the order of 100 μm were required to initiate the development of karstic conduits [Groves and Howard, 1994a]. Large initial variations in fracture aperture led to the development of preferentially enlarged karstic conduits with irregular paths [Groves and Howard, 1994b]. With a transition to turbulent flow they observed a more uniform development of karstic channels [Howard and Groves, 1995]. Dreybrodt [1996] and Siemers and Dreybrodt [1998] have used 1- and 2-D percolation networks to assess the effect of the width of initial fracture aperture distributions on karstic breakthrough times.

Additionally, there have been a number of studies in porous rather than fractured rock that have described the development of porosity during acidization of carbonate reservoirs and the closure of porosity due to cementation. *Hoefner and Fogler* [1986, 1988] developed a model, based on a two dimensional triangular lattice, to investigate the evolution in pore size distribution with dissolution. *Daccord et al.* [1989] and *Lauritzen et al.* [1992] used a similar model to study 'wormholing' phenomena associated with the acidization of hydrocarbon production boreholes. *Daccord*, [1987] and *Daccord and*

Lenormand [1987] used diffusion-limited aggregation models to investigate the patterns of dissolution during reservoir acidization. Roberts and Schwartz [1985] and Wong et al. [1984, 1986] considered porosity reduction due to cementation using a three dimensional network of tubes: the conductance being proportional to the fourth power of the radius and the rate of change of radius being (effectively) proportional to the radius.

2.2 Rationale of the Present Study

The motivation for the present work is to develop a model to simulate the geometry of preferentially enlarged (sub-karstic) fractures in the Chalk, an important carbonate aquifer over large areas of northwest Europe [Downing et al, 1993]. Unlike the previously described studies of reactive transport, karst formation and reservoir acidization, we have not adopted a process-dependent approach. Instead, we have chosen to adopt a generic approach, as described below. The aim of this approach is to provide a modelling 'engine' and develop methodologies that will generate realistic porosity templates for use in flow and transport models of fractured aquifers such as the Chalk. However, we foresee that the model may also be applicable to a wide range of other geological scenarios.

Although it is known that transport in the Chalk is dominated by flow through a well connected network of enlarged fractures [Price, 1987; Barker, 1993; Price et al., 1993], little is known about the detailed geometry of the fracture network or of flow channelling in the aquifer, and, specifically, there is little information on aperture distributions [Bloomfield, 1996]. In addition, there are uncertainties associated with the detailed timing and rate of formation of the preferentially enlarged fractures. It is thought that the principal process of fracture enlargement in the Chalk is dissolution [Price, 1987; Price et al., 1993]. However, present-day recharge is essentially fully saturated by the time it has passed through the soil zone [Edmunds et al, 1992], thus limiting the potential for significant presentday dissolution. It has been suggested that much of the development of the enlarged fractures occurred during periglacial episodes when recharge waters were relatively cool and more chemically aggressive with respect to contemporary recharge [Younger, 1989]. The removal of cover rocks and the development of stable discharge points following the last glaciation, and the consequent concentration of flow to those discharge points, have also been suggested as mechanisms for localised enlargement of parts of the fracture network [Price et al., 1993; Lloyd, 1993]. Mechanical weathering and biologically mediated geochemical processes may also be significant factors over geological time-scales and may contribute to the enlargement of shallow fractures. Given the many uncertainties associated with the likely processes of fracture aperture growth, we have adopted a simple geometric, process-independent, modelling approach to the study of fracture aperture development.

Normally stochastic network models used to generate 'realistic' fracture networks only contain local information as they are based on single-fracture statistics (e.g. distributions of fracture density, size, aperture, and orientation). Such models are unlikely to exhibit the long-range preferential pathways that are important for contaminant transport. Some modelling has recently been done with fractal networks [Acuna and Yortsos, 1994], which are more likely to include long-range pathways although they need not be responsible for a significant proportion of the flow. The simulated annealing approach of Long et al. [1991] is a promising development in which a network is adjusted in order to honour observational data. This method does have the potential to result in models which exhibit long-range preferential paths given (a) suitable data (e.g. long-range tracer results) and (b) a suitable template for the fracture network. A specific task of this study is to be able to model the long-range preferential pathways that are thought to occur naturally in fractured aquifers such as the Chalk.

We have investigated patterns of fracture aperture growth given simple growth laws applied to fracture arrays with simple initial aperture distributions. Our approach is therefore in the spirit of statistical mechanical studies of simple systems such as percolation models [Berkowitz and Balberg, 1993; Sahimi, 1994; Stauffer and Aharony, 1994]. The objective of this type of study is to reveal general characteristics of behaviour (e.g. geometrical phase transitions) ahead of studies of behaviour

in relation to specific processes with their individual magnitudes and time scales. The formulation given for the problem is therefore generic, and the parameters have no absolute values: it is best to think of each parameter (e.g. time) as a dimensionless variable equal to the real time divided by a characteristic time for the specific processes under consideration. *Sahimi et al.* [1990] and *Sahimi* [1995] distinguish two approaches to modelling diagenetic processes: continuum and geometric modelling. In 'continuum modelling' the equations describing reaction and transport are solved to provide average behaviour. 'Geometric modelling' is based on a model of the pore space and makes simplified assumptions about the development of the porosity. Our work falls into the latter category of investigation.

The paper is organised as follows. First we present a description of EVOLVER, the fracture aperture growth model. This includes a discussion of the underlying assumptions, the mathematical formulation and a description of how the model is implemented. We also describe the range of variables that have been investigated. In the absence of appropriate geometrical parameters to characterise the diverse and complex aperture arrays that develop, the results are presented graphically and are characterised using only simple statistical measures. The results are then discussed in the context of geometrical phase changes in simple systems, and the conductivity of the evolved fracture aperture arrays is investigated using a continuum percolation model. Some of the limitations of the aperture growth model are also discussed. Finally, some of the requirements for the quantitative description of dynamic systems are outlined.

3. THE MODEL

A number of assumptions underlie the EVOLVER model. It is helpful to separate the 'generic' assumptions, that we feel would apply to a broad class of systems similar to that which we have studied, from the 'specific' assumptions in the implementation (as the current version of EVOLVER) for which we present and discuss results.

Generic assumptions:-

- A. The fracture system is connected: there is a pathway from every fracture to every other fracture.
- B. The characteristic time for hydraulic equilibrium to be established across the systems is negligible in relation to the rates of change of the apertures and (hence) the fracture conductivities. (Therefore the system is always in a quasi-steady-state of flow.)
- C. The fractures consist of finite sections over which the aperture is uniform. So, without loss of generality, we consider each fracture to be one section of constant aperture.
- D. The rate of change of fracture aperture depends only on the aperture and the rate of flow through the aperture. (The direction of flow is not important.)
- E. The volumetric flow rate along each fracture is a function of the head gradient and aperture.

Specific assumptions:-

- 1. The initial distribution of apertures is random, uncorrelated and conforms to a known (normally lognormal) distribution.
- 2. The rate of change of apertures is a polynomial function of the aperture and flow rate.
- 3. Darcy's law applies so conductivity depends only on the apertures.
- 4. The fractures are of equal length on a square grid (Figure 1).
- 5. Flow in the grid is controlled by no-flow boundary conditions on two opposite edges and either: (a) a fixed head difference between the other two edges, or (b) a variable head difference between the other two edges maintained so as to give a fixed total flux (Figure 1).
- 6. There is no head loss at fracture intersections.

3.1 Mathematical Description of the Model

While the conceptual model is relatively straightforward, this is somewhat awkward to express in precise mathematical terms. The following might be skipped at first reading.

We envisage a set of N fractures that make connections across a set of M nodes. With each fracture, i, we associate a pair of nodes (j,k). We allow there to be more than one fracture between two nodes (although in the present study we only use single fractures between nodes arranged in an orthogonal grid, Figure 1), so it is best to think of the pair (j,k) as determined by i but not vice versa. We cannot order the pair according to flow direction as that is not known a priori and may change over time.

Figure 1. Boundary conditions for the EVOLVER model.

From assumption 4, for each of the *N* fractures the rate of change of aperture is given by:

$$\frac{da_i}{dt} = G(a_i, v_i, \mathbf{p}^G) \quad i = 1, ..., N$$
(1)

where a_i is the aperture in fracture (or fracture section) i, t is time, \mathbf{p}^G is a set of parameters, and v_i is the magnitude of the volumetric flow rate in fracture i:

$$v_i = \left| v_{jk}^i \right| \tag{2}$$

where v_{jk}^i is the volume of flow per unit time from node j to node k through fracture i. (A specific example of the fracture growth function, G, is given later as Equation (9).)

The set of initial apertures $\mathbf{a_0} = \{a_{10}, ..., a_{N0}\}$ is assumed known:

$$a_i(0) = a_{i0}$$
 $t = 0$, $i = 1,...,N$ (3)

From assumption 3, the volume of flow from node j to node k through fracture i is given by the conductivity of fracture i times the head gradient

$$v_{jk}^{i} = \mathbf{K}(a_{i}, \mathbf{p}^{K}) \frac{h_{j} - h_{k}}{L_{i}}$$

$$\tag{4}$$

The fracture is characterised by its length L_i and the value of the 'conductivity' function, K, which depends on the specific aperture and a general set of parameters, \mathbf{p}^K .

Equation (3) can be generalised to

$$v_{jk}^{i} = V(a_i, v_i, (h_j - h_k) / L_i, \mathbf{p}^{V})$$

$$(5)$$

where V is a function involving a set of parameters, \mathbf{p}^V . This form could accommodate, for example, the Forchheimer equation for non-darcian flow.

The head differences across the fractures are given by the solution of the mass balance equation. The net flow into any node (fracture intersection) is zero:

$$\sum_{i} v_{jk}^{i} = 0 \quad \forall j \tag{6}$$

where, for a given node, j, we sum over all connected fractures, i, each of which identifies the connecting node, k, uniquely. As we allow the possibility of more than one fracture connecting two nodes, (a) there is no redundancy in using the three indices i, j and k, and (b) nodes j and k do not uniquely identify fracture i.

Assumption (5a) gives the boundary conditions needed for the solution of Equation (6):

$$h_n = \begin{cases} H & n \in \aleph_u \\ 0 & n \in \aleph_d \end{cases} \tag{7}$$

where \aleph_u and \aleph_d are the sets of upstream and downstream (fixed-head) nodes, respectively. We can set the head difference H to unity when we have a fixed-head boundary conditions or determine H such that the required flux is unity (assumption 5b).

Note that no-flow conditions are not specified explicitly since they arise naturally in relation to the (lack of) connectivity of the system.

In summary, the complete set of apertures for all fractures, \mathbf{a} , can formally be regarded as a function, A, of the parameters:

$$\mathbf{a} = \mathbf{A}(t, \mathbf{a}_0, \mathbf{L}, \mathbf{p}^G, \mathbf{p}^K, H, \aleph_u, \aleph_d)$$
(8)

where L is the set of fracture lengths. So the central task is to evaluate this time-dependent function from Equations (1) to (7)

3.2 Numerical Implementation within the EVOLVER Code

It is important, both conceptually and from a practical point of view, to understand the nature of the mathematical problem posed in the above equations. Essentially the task of computing the aperture development is an 'initial value problem': expressed by a set of N first order equations, Equation (1), subject to the initial aperture values, Equation (3). To solve these equations we must evaluate the function G in Equation (1). This in turn involves the evaluation of volume flow rates from Equation (4) and this requires the solution of the set of equations expressed in Equation (6). (That solution of Equation (6) is equivalent to solving the finite-difference formulation of the Laplace equation in conventional groundwater flow problems where it is the central task: here that task is subsidiary.)

The solution of Equation (1) has been implemented using a Runge-Kutta method although any standard method should work adequately. The time steps are varied by that method in order to attain a specified accuracy but output of results was specified to be at regular time intervals, which is achieved but shortening time steps, if necessary.

Thus far we have only considered fractures forming a two-dimensional square grid. However, the formulation of the problem puts no restriction on geometry. This allows solution of Equation (6) - a set

of linear equations - using an iterative (LSOR) relaxation method. This has worked well since a good estimate of the solution is known from the previous time step except initially. For the case of a fixed head difference across the whole fracture system, the upstream head can be specified relative to a zero downstream head without loss of generality.

For the case of a constant flux, a complication arises since we do not know *a priori* the head difference that is needed to give a chosen flux. When we take the flux proportional to the head difference, as in Equation (3), then this is not a problem as all volumetric flow rates scale with the head difference. We therefore compute flow based on a zero downstream head and a unit upstream head. We then calculate the flux through the system and scale all heads by a factor equal to the ratio of the required total flux and the flux obtained with unit head difference. To implement Equation (5), expressing non-darcian flow, would require an iterative evaluation of the head; this has not yet been implemented in EVOLVER.

The code we have developed thus far expresses the functions G and K as polynomials:

$$G(a_{i}, v_{i}, \mathbf{p}^{G}) = \left(\sum_{m} b_{m} a_{i}^{c_{m}}\right) \left(\sum_{m} d_{m} v_{i}^{e_{m}}\right) i = 1, ..., N$$
(9)

$$K(a_i, \mathbf{p}^K) = \sum_{m} f_m a_i^{g_m} \quad i = 1, ..., N$$
 (10)

so the parameter sets are, in this particular case,

$$\mathbf{p}^{G} = \{b_{1}, b_{2}, \dots, c_{1}, c_{2}, \dots, d_{1}, d_{2}, \dots, e_{1}, e_{2}, \dots\}$$
(11)

$$\mathbf{p}^{K} = \{f_{1}, f_{2}, \dots, g_{1}, g_{2}, \dots\}$$
 (12)

This allows a reasonable amount of flexibility while obviating the need to recompile the code. The parameters become part of the data set read in during each run. However, equations (9) and (10) are readily replaced in the code and there is little restriction on their form or complexity.

In practice the initial aperture distribution is set at the start of each model run as are the parameters in Equations (11) and (12). EVOLVER evaluates heads and flow rates throughout the fracture array according to Equations (6), (7) and (4), and new fracture apertures are then calculated from Equation (1). These new calculated apertures are taken to be the aperture distribution at time one and are used as input in the next iteration of the model. The model is iterated to a specified time, and head, flow rate and aperture data are recorded for each fracture at each time.

3.3 Range of Investigation

The EVOLVER code has been designed so that the boundary conditions, including the initial aperture distribution and the functional form of the aperture growth-rate law are all flexible. However, in order to investigate systematically the growth of fracture aperture distributions using the model, and to avoid generating unmanageable quantities of data, it was necessary to restrict our range of investigation. All tests were performed on 20×20 arrays of fractures arranged on an orthogonal (square) lattice, Figure 1. A 2-D lattice was chosen to save on computational time and because it was easier to represent the results graphically. The natural fracture growth processes that we are modelling occur in 3-D and it is expected that any trends in the geometry of the evolved arrays, particularly geometrical phase transitions, identified in 2-D will also occur in 3-D. However, by analogy with percolation theory, we expect any geometrical phase changes to occur at different thresholds in 2- and 3-D. For example, *Silliman* [1990] demonstrated the well-known percolation

theory results that lattice geometry significantly influences the site percolation threshold p_c , i.e. $p_c = 0.312$ in 3-D and $p_c = 0.593$ in 2-D [Berkowitz and Balberg, 1993].

Each model run described in this paper was performed with a constant unit flux condition across the lateral boundaries and a no-flow condition at the upper and lower boundaries, Figure 1. Limited tests under conditions where a constant head was applied across the array appeared to produce qualitatively similar aperture arrays to those generated by constant flux conditions. However, large apertures developed rapidly after only a few time units. The model was generally much less robust under constant head conditions and the code was liable to crash at very early times, due to difficulties in obtaining a stable solution for Equation (6). In addition, the constant flux condition was favoured as it was generally thought to be more realistic when considering the long-term evolution of fracture networks in groundwater catchments. Because the system is always in a quasi-steady-state of flow (generic assumption B), and as there is no tracking of 'packets' of water through the fracture array, the model is symmetrical. Model runs using identical initial aperture distributions with constant fluxes from left to right and from right to left developed identical evolved aperture arrays.

Although EVOLVER allows flexibility in the form of the initial aperture distribution, there is only limited information available on natural fracture aperture distributions that can be used for conditioning the model. The topography of joint surfaces has been studied in detail using profilometers [*Brown and Scholz*, 1985b] and has been shown to be essentially fractal in nature for a range of rock types, however, there are few direct measurements of fracture aperture distributions. *Hakami and Barton* [1990] fitted lognormal distributions to aperture distributions measured in joints in a variety of coarse-grained igneous and metamorphic rocks. *Moreno et al.* [1988] reported on the work of Bianchi and Snow and Bourke *et al.* who found that aperture distributions derived from core and well logs and permeability tests in granites follow lognormal distributions. Generally, modelling studies of transport in single fractures and in fracture networks assume a lognormal aperture density distribution [*Moreno et al.*, 1988; *Tsang et al.*, 1988; *Nordqvist et al.*, 1992], although *Tsang and Tsang* [1987] used a Gamma function. *Bloomfield* [1996] has reported a bi-modal aperture distribution from a single bedding plane fracture in Chalk where the larger apertures were lognormally distributed and were inferred to be associated with solution enlarged components of the fracture.

The present study uses a lognormal aperture distribution for the initial array. A limited number of model runs were performed using an exponential distribution of apertures in the initial array. The results of these runs appeared to be qualitatively similar to those based on lognormal initial distributions. The model has also been restricted so that the initial apertures are spatially uncorrelated. Consequently, any spatial correlations in the evolved aperture arrays will be due solely to self-organisation arising from the aperture growth process.

The model was used to investigate the dependence of aperture geometry on the breadth (standard deviation) of the initial aperture distribution, and on the form of simple aperture growth-rate laws. It was not used to investigate the effects of the mean initial fracture aperture on evolved fracture aperture distributions. Consequently, all the runs described in the present study had initial lognormal aperture distributions with means, a_0 , of $\log_{10} 0$. The standard deviation of the initial lognormal aperture distribution, σ_{a0} , was investigated in the range $\log_{10} 0.1$ to $\log_{10} 0.7$, and most runs where performed with an initial standard deviation of $\log_{10} 0.3$. Log₁₀ 0.3 was adopted as the default value because, for an initial mean aperture of $\log_{10} 0$, and for the range of times investigated, (i) it produced a range of evolved fracture apertures (about three orders of magnitude) that could be represented graphically in fracture maps without recourse to graphical log-scales, and (ii) it was possible to map out a range of evolved structures and identify geometrical phase changes. The fracture aperture maps, for example Figure 2, show the spatial distribution of apertures in the network where line thickness is proportional to the calculated aperture of each evolved fracture. The separation of nodes in the fracture aperture maps, has been fixed at an arbitrary length scale, so that the evolved apertures, which also have an arbitrary width scale, do not overlap in the graphical presentation.

Only the most simple aperture growth laws were tested. The aperture growth-rate was restricted to a first order polynomial function of flow rate in Equation (9), and was taken to be independent of aperture, i.e. Equation (1) was reduced to

$$\frac{da_i}{dt} = (v_i)^e i = 1, \dots, N \tag{13}$$

The aperture growth-rate exponent, e, was investigated in the range 0.1 to 0.8. Most of the runs have been performed assuming plane fracture flow, i.e., f was set to 1 in Equation (10) to give

$$K_i = (a_i)^g i = 1, ..., N$$
 (14)

and g was set to 3. However, a few runs were performed with g in the range 2 to 3 to investigate the affect of deviations from 'cubic law' behaviour [Barker, 1993] on the evolved structures.

4. RESULTS

The influence of the aperture growth-rate exponent, e, on evolved aperture geometry is illustrated in Figures 2 and 3. Figure 2 consists of six fracture aperture maps (after a time of 100) for growth-rate exponents between 0.2 and 0.7. Each run shown in Figure 2 was performed on statistically equivalent initial aperture distributions, i.e., $a_0 = \log_{10} 0$ and $\sigma_{a0} = \log_{10} 0.3$. Run 35 shows the homogeneous enlargement of apertures parallel to the flow direction (row apertures) given a low aperture growth-rate exponent of 0.2. Fracture apertures perpendicular to the flow direction (column apertures) are also relatively uniformly developed, but have smaller apertures than the row apertures. An aperture map generated using a growth-rate exponent of 0.3, run 29, shows a slightly more heterogeneous row aperture structure, and an apparently slightly lower average row aperture than run 35, but it exhibits a similar overall geometry.

Maps of evolved fracture arrays for aperture growth-rate exponents of 0.4, 0.5 and 0.6, runs 30, 27 and 32 respectively, show relatively complex geometries. These fracture arrays consist of diverging and joining channel-like paths of preferentially enlarged row apertures sub-parallel to the flow direction that are connected by relatively short steps of enlarged column apertures. At higher growth-rate exponents there are fewer, but more pronounced, preferentially enlarged channel-like paths. The enlarged aperture paths, particularly at higher growth-rate exponents, by-pass regions of the fracture array containing both row and column apertures that have undergone relatively little growth, e.g. the centre left-hand edge and the bottom right-hand corner of the map corresponding to run 32. At an aperture growth-rate exponent of 0.6, run 32, a dominant, preferentially enlarged, bifurcating path has almost developed, and at an aperture growth-rate exponent of 0.7, run 34, a continuous channel-like path of preferentially enlarged apertures develops that spans the array. There are two small by-pass structures associated with the array-spanning path in run 34, but the apertures in these and the preferentially developed path are all significantly larger than the other fractures in the array.

Figure 3 shows four lognormal probability plots of fracture aperture data for arrays generated with aperture growth-rate exponents 0.2, 0.4, 0.6 and 0.8. Each run shown in Figure 3 was performed on statistically equivalent initial aperture distributions, i.e. $a_0 = \log_{10} 0$ and $\sigma_{a0} = \log_{10} 0.3$. Additional runs performed on aperture arrays with both statistically and spatially identical initial aperture distributions showed the same trends as those seen in Figure 3, indicating that the trends are independent of the initial spatial distribution of apertures. Five aperture populations are shown in each lognormal probability plot, corresponding to the initial aperture distribution and the distributions at time 100, 200, 300 and 600.

Run 50 shows the development of two aperture sub-populations associated with an aperture growthrate exponent of 0.2. The larger, approximately constant, aperture values are associated with the row apertures, the smaller column apertures remain lognormally distributed as the array evolves. All fracture apertures have grown significantly by time 100 (by up to two orders of magnitude) with the rate of aperture growth slowing after time 100. Run 30 shows the development of fracture apertures for an aperture growth-rate exponent of 0.4. There is a continuum of fracture apertures that departs from a lognormal distribution, and although at a given time the growth of the largest apertures is of a similar magnitude to that seen for an aperture growth-rate exponent of 0.2, the smaller apertures undergo little growth after time 100. For an aperture growth-rate exponent of 0.6, run 32, the smallest apertures undergo little growth even by time 100 and appear pinned near their initial values. The largest apertures continue to grow at only a slightly greater rate than those with growth-rate exponents of 0.2 and 0.4, however, there are relatively of few of these large apertures at the higher growth-rate exponent. The largest apertures in runs 30 and 32 predominantly correspond to the preferentially enlarged row apertures. Two discontinuous aperture populations develop with a growth-rate exponent of 0.8, run 33. The largest apertures are associated with a single continuous array-spanning path of preferentially enlarged apertures. These apertures continue to develop after time 100.

Figure 2. Maps showing the effect of variations in the aperture growth-rate exponent on the form of evolved aperture arrays. Runs 35, 29, 30, 27, 32 and 34 correspond to aperture growth-rate exponents 0.2, 0.3, 0.4, 0.5, 0.6 and 0.7 respectively. Each map is based on an initial aperture distribution with a mean of $\log_{10} 0$ and σ_{a0} of $\log_{10} 0.3$, where all the maps show the evolved structure at time 100.

Figure 3. Lognormal probability plots of aperture data for maps generated with aperture growth-rate exponents 0.2, 0.4, 0.6 and 0.8 (runs 50, 30, 32 and 33 respectively). All runs were performed on an initial aperture distribution with a mean of \log_{10} 0 and σ_{a0} of \log_{10} 0.3. Five aperture populations are shown in each probability plot, corresponding to the initial aperture distribution and distributions at times 100, 200, 300 and 600.

All other apertures are essentially unchanged after time 100 having undergone little or no growth from their initial apertures.

A characteristic feature of the aperture distributions that develop at a growth-rate exponent of 0.6, run 32, are the small approximately lognormal sub-populations in the data at larger apertures. These appear to be associated with the detailed structure of the dominant aperture path. Figure 4 shows a normal probability plot and corresponding aperture map for run 40 (e = 0.6 and $\sigma_{a0} = \log_{10} 0.3$ at time 100) where three sub-populations can be differentiated. The main array-spanning path consists of the most preferentially enlarged apertures (triangles in the probability plot). These fractures have an approximately constant aperture. The second sub-population, the splays and by-pass structure on the main array-spanning path (diamonds), consist of fractures with relatively large but variable apertures. The remaining apertures (circles) are associated with fractures away from the enlarged aperture path.

Figure 4. Illustration of the development of aperture sub-populations given an aperture growth-rate exponent of 0.6 ($\sigma_{a0} = \log_{10} 0.3$ and t = 100). The lognormal probability plot shows three approximately lognormal aperture sub-populations.

Figures 5 and 6 illustrate the effect of variations in σ_{a0} on the geometry of the preferentially enlarged paths that develop at high aperture growth-rate exponents (in these examples for an aperture growthrate exponent of 0.7). Figure 5 consists of six fracture aperture maps generated using values of σ_{a0} in the range $\log_{10} 0.1$ to $\log_{10} 0.6$. Each map illustrates the array after time 100. Figure 5 shows that for $\sigma_{a0} = \log_{10} 0.1$ a single straight array-spanning path develops. As σ_{a0} increases up to about $\log_{10} 0.5$ the preferentially enlarged array-spanning path becomes more tortuous. Above about $\log_{10} 0.5$ the tortuosity of the preferentially enlarged paths decreases. Figure 6 is a plot of tortuosity as a function of σ_{a0} , where tortuosity, τ , is defined as $(L_e/L)^2$, and where L_e is the effective path length and L is the direct path length [Dullien, 1979]. Where there are by-pass structures on the preferentially enlarged path the tortuosity was measured along the path of the largest aperture. Figure 6 shows a maximum tortuosity of about three at about $\sigma_{a0} = \log_{10} 0.5$. Figure 5 also shows that at very high values of σ_{a0} enlarged isolated apertures begin to develop away from the dominant path. At times of the order of 100 the model becomes unstable for σ_{a0} greater than $\log_{10} 0.7$. This is due to difficulties in obtaining a stable solution for Equation (6). However, runs to small times before the model becomes unstable suggest that at very high values of σ_{a0} the continuous enlarged array-spanning path breaks down and isolated fractures away from the path become highly enlarged.

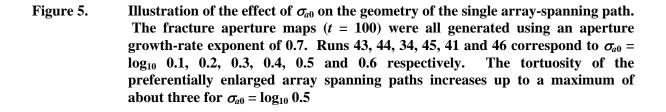


Figure 6. Variation in tortuosity as a function of σ_{a0} .

4.1 Evolution in Transmissivity as a Function of Aperture Growth-rate

The evolution in effective transmissivity, T_{eff} , of the developing fracture arrays can be followed by monitoring changes in head differences across the fracture arrays. Where effective transmissivity is given by

$$T_{eff} = Q/\Delta H \tag{15}$$

and where Q is the bulk flux across the fracture array and ΔH is the head difference parallel to the direction of flux. Figure 7 shows variations in the effective transmissivity of six fracture arrays with aperture growth-rate exponents in the range 0.2 to 0.7 up to time 100 ($\sigma_{a0} = \log_{10} 0.3$ and $a_0 = \log_{10} 0$). The results are plotted on a \log_{10} - \log_{10} scale. All the fracture arrays exhibit a power-law like growth in effective transmissivity with respect to time. The arrays with the lowest aperture growth-rate exponents (e = 0.2 and 0.3) exhibit the most significant absolute increase in transmissivity with time. Such that after time 100 the effective transmissivity of the array with an aperture growth-rate exponent of 0.2 is over an order of magnitude greater than the similar array with a growth-rate exponent of 0.7. This is because even though the apertures of the preferentially enlarged array spanning paths are slightly larger than the equivalent row apertures in the arrays with low growth-rate exponents (Figure 3), enlarged apertures develop in all row-parallel fractures at low growth-rate exponents (Figure 2).

Figure 7. Variation in effective transmissivity of six fracture arrays with aperture growthrate exponents in the range 0.2 to 0.7 up to time 100 ($\sigma_{a0} = \log_{10} 0.3$ and $a_0 = \log_{10} 0$).

5. DISCUSSION

A number of basic features of the evolved fracture aperture arrays have been described in the previous section. These can be summarised as follows,

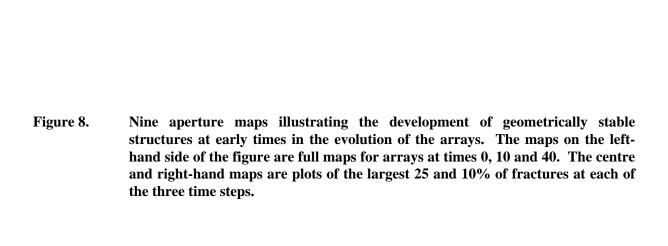
- 1. evolved structures are highly sensitive to initial boundary conditions,
- 2. for the range of initial boundary conditions considered, aperture distributions appear to be statistically stable by a time of 100,
- 3. diverse structures develop; ranging from the relatively uniform development of row-parallel apertures to the development of preferentially enlarged single array-spanning paths,
- 4. the tortuosity of the preferentially enlarged array-spanning paths is a function of the breadth of the initial aperture distribution, and
- 5. effective transmissivity of the arrays increases in a power-law like manner as a function of time.

In this section we discuss how structures may evolve before time 100, and how the statistically stable structures may develop. We investigate geometrical phase changes in the evolved arrays as a function of the initial boundary conditions. We also consider whether methods such as critical path analysis can be used to predict the effective transmissivity of the arrays. This section is concluded with a discussion of the limitations of the current EVOLVER model and the approach that we have adopted, and a brief discussion of the requirements for a quantitative description of the properties of dynamic systems and structures such as those generated by EVOLVER.

5.1 Structural Evolution in the Fracture Aperture Arrays

Figure 3 shows that the form of the evolved fracture aperture distribution appears to be fixed by time 100, regardless of the aperture growth-rate exponent. After time 100 the aperture distribution is simply amplified (on an approximately logarithmic scale). However, it is not clear from Figure 3 whether the stable form to the aperture distribution corresponds to stable geometrical configurations or evolving geometrical configurations with statistically stable aperture distributions, and if the geometrical configuration is stable, how this develops prior to time 100. The changes in the effective transmissivity of the array, Figure 7, do not provide any insight into these questions.

Figure 8 presents nine aperture maps for evolved fracture arrays based on the following run conditions, $a_0 = \log_{10} 0$, $\sigma_{a0} = \log_{10} 0.3$ and e = 0.5. The maps on the left-hand side of the figure are the full fracture aperture maps for arrays at time = 0 and after times 10, and 40. In the centre and righthand columns only the largest 25 and 10 % of apertures respectively are plotted for each time. The figure demonstrates that at an early stage in the evolution of the array, the largest apertures are distributed throughout the array and may have both row- and column-parallel orientations. As the array develops the largest fracture apertures coalesce to form more continuous structures. They form an increasingly anisotropic fabric, which at higher aperture growth-rate exponents, leads to the development of the preferentially enlarged array-spanning paths. As a consequence of the clustering of the larger fracture apertures and an increase in their anisotropy, at latter times fewer relatively large aperture fractures are required to contribute to the formation of the array-spanning path. Based on Figure 8, it is inferred that the re-organisation of the largest fracture apertures corresponds to the formation of geometrically (and statistically) stable aperture distributions. There is no evidence for switching of preferential aperture growth between two or more array-spanning structures during the early development of the array, and it is inferred that once formed the structures evolve in a stable manner.



The formation of geometrically stable aperture distributions is also reflected in the variations in flow rate within different components of an evolving fracture array. Based on fracture aperture data from run 58 that developed an array with a preferentially enlarged array-spanning structure ($a_0 = \log_{10} 0$, $\sigma_{a0} = \log_{10} 0.3$, and e = 0.6), Figure 9 shows variations in flow rate from nine selected fractures. The closed circles represent flow rate changes in seven representative fractures away from the array spanning structure with a range of initial aperture distributions. The open triangles show the flow rate changes in the fracture with the smallest aperture that is part of the preferentially enlarged array-spanning structure at time 100, the 'critical fracture', with a critical aperture, a_c . The open circles show the change in flow rate in the fracture with the largest aperture (also part of the array-spanning structure). The fractures away from the array spanning structure show a range of flow rate histories. Fractures with smaller initial apertures generally exhibit a decline in flow rate with time; the fractures with larger initial apertures show a small increase in flow rate before flow rate declines. Flow rates in both the largest fracture in the array-spanning path and in the critical fracture always increase, although they appear to tend towards an asymptote at time o100.

Figure 9. Examples of changes in flow rate with time in selected fractures during the early stages of growth of an array where an array-spanning structure develops.

The largest fracture aperture (at time = 100) that is not part of the array-spanning structure, fracture 13 in Figure 9, is located near the critical aperture and near the array spanning structure. Flow rate in fracture 13 is at a maximum at about time = 60, at the same time as the flow rate in the critical aperture exceeds the maximum flow rate in this fracture. These changes in flow rate in the two fractures are interpreted as representing local competition for flow and may indicate that flow is 'scavenged' by the critical aperture and into the array spanning structure as it develops. For the particular fracture array under consideration, some fractures show stable development from time = 0, i.e. a continuos reduction in flow rate, but for the array as a whole the distribution of flow (and hence structural development) is subject to transient changes up to about time = 60. The example in Figure 9 is intended only as an illustration of the transient behaviour of the arrays before their structures stabilise. Arrays corresponding to other initial boundary conditions may stabilise more or less quickly.

5.2 Geometrical Phase Transitions in the Evolved Aperture Arrays

Phase transitions are characteristic of many simple systems, e.g. the magnetic behaviour of a material near its Curie point or the physical state of a material near its liquid-gas critical temperature. At a phase transition, a system changes its behaviour qualitatively at one particular value of a continuously varying parameter. Within the system we have been studying, can we recognise any geometrical phase transitions as a function of the initial boundary conditions, particularly as a function of the aperture growth-rate

exponent? For example, can we identify any changes in the fracture arrays shown in Figures 2 and 5 as a function of the growth-rate exponent?

Although Figure 3 shows distinct differences in the evolved aperture distributions given different aperture growth-rate exponents, the evolved aperture maps in Figure 2 are difficult to interpret. Due to the extreme diversity of the evolved structures it is hard to identify a single factor that will adequately characterise all the evolved aperture arrays. However, we have chosen the standard deviation of row apertures, σ_{row} , to characterise the fracture networks. This is because a common feature of all the evolved arrays is their increased symmetry with respect to the flow direction relative to the initial aperture distribution (row apertures are generally enlarged and column generally apertures poorly developed). It provides a rough measure of the degree of self-organisation, or emergence, in the evolved arrays. Figure 10 is a plot of σ_{row} against aperture growth-rate exponent and time. It is based on times up to 1000 for the six runs shown in Figure 2, and for run 33 shown in Figure 3 (i.e. for aperture growth-rate exponents in the range 0.2 to 0.8). The data have been contoured to highlight the trends in the surface.

Figure 10. Plot of σ_{row} against aperture growth-rate exponent and time (up to 1000) for the six runs shown in Figure 2, and for run 33 shown in Figure 3. The data have been contoured to emphasise the trends in the surface. Three geometrical regimes are indicated.

Figure 10 shows three structural regimes separated by two geometrical phase changes. In regime 1, at aperture growth-rate exponents less than or equal to about 0.3, σ_{row} falls rapidly at early times. This regime is characterised by a homogenisation of row apertures with time. In regime 2, at aperture growth-rate exponents in the approximate range 0.3 to 0.6, row apertures become increasingly heterogeneous with both time and with higher growth-rate exponents. In regime 3, at aperture

growth-rate exponents greater than about 0.6, row aperture heterogeneity increases with time for a constant growth-rate exponent, but appears to drop sharply at constant time with increasing growth-rate. Other geometrical regimes, and hence other geometrical phase boundaries, may be present outside the range of investigation. For example, the transition to isolated enlarged apertures at high σ_{a0} and at high values of e has already been inferred, see Figure 5. Additionally, it is possible to envisage boundary conditions that would lead to the growth of all fracture apertures proportional to their initial aperture distribution, i.e. maintaining a lognormal aperture distribution where the geometric mean aperture increased linearly with time.

Changes in the tortuosity of array spanning paths as a function of σ_{a0} , Figures 5 and 6, suggests that geometrical phase changes identified in Figure 10 may be extended into $e/t/\sigma_{a0}/\sigma_{row}$ space. In addition, limited modelling at initial mean apertures other than \log_{10} 0, has shown that lower initial mean apertures lead to the promotion of single array spanning paths at constant σ_{a0} , and that higher initial mean apertures lead to more heterogeneous, but relatively isotropic, structures, Figure 11. This observation, and comparison of Figures 2, 5, and 11 also suggests that the form of evolved aperture arrays will not scale simply as a function of the a_0/σ_{a0} ratio. It is inferred from these observations that it may be possible to map out geometrical phase changes similar to those seen in Figure 10 in $e/t/\sigma_{a0}/\sigma_{row}/\sigma_{a0}$ space.

Figure 11. Three aperture maps illustrating the effect of a_0 on the form of evolved aperture arrays. All fracture maps were generated using an aperture growth rate exponent of 0.6 and using $\sigma_{a0} = \log_{10} 0.3$. Figure 11a was generated using an initial mean aperture of $\log_{10} 1$, and Figures 11b and 11c using initial mean apertures of 0 and 1 (runs 48, 37 and 47 respectively).

All the runs that have been described so far were generated assuming plane fracture flow through individual fractures, i.e. flow rate was taken to be proportional to the cube of the aperture [Barker, 1993] (g=3 in Equation 14). This was thought to be reasonable given the uniform fracture aperture assumption (assumption C). A limited number of runs were performed with values of g in the range 3 to 2 to assess the affects of relaxing the 'cubic law' condition. It was found that higher values of g tend to promote the development of preferentially enlarged, array-spanning, aperture paths, and that lower values of g tend to lead to more homogeneous enlargement of fracture apertures parallel to the head gradient. Consequently, the position of geometrical phase changes in $e/t/\sigma_{a0}/\sigma_{row}/a_0$ space are also sensitive to the relationship between fracture aperture and flow rate.

The phase changes in Figure 10 are poorly defined because they are based on a limited number of realisations, where each realisation is associated with a degree of uncertainty. The effects of these uncertainties may be particularly pronounced near geometrical phase transitions. This is illustrated in

Figure 12, which shows σ_{row} against t curves for realisations using an aperture growth-rate exponent of 0.6 and for a value of σ_{a0} of \log_{10} 0.3. The solid circles are mean values of σ_{row} based on fourteen independent runs (error bars are 1 S.D.). The runs with maximum and minimum evolved values of σ_{row} are shown separately. Run 98 shows the highest values of σ_{row} . It is not associated with a single array-spanning preferentially enlarged aperture path, but shows a number of anastomosing enlarged aperture paths. Run 32 has the lowest evolved value of σ_{row} and shows a single, well developed, preferentially enlarged array-spanning path. It can be seen from inspection of Figures 10 and 12 that multiple realisations would be necessary to reduce uncertainty in identifying and characterising the position of the geometrical phase transitions.

Figure 12. Illustration of the uncertainties in characterising the form of aperture arrays near a phase change boundary. The plot shows how σ_{row} varies with time for an aperture growth-rate exponent of 0.6 and σ_{a0} of \log_{10} 0.3. The solid circles are mean values based on fourteen independent realisations (error bars 1 S.D.). Runs with the maximum and minimum evolved values of σ_{row} are also shown, as are their corresponding aperture maps.

What is the physical meaning of the geometrical phase changes illustrated in Figure 10? There are only a limited number of patterns that can be produced by lines connecting regular nodes on a 2-D plane. Stevens [1974] showed how different patterns of connectivity were related to total path length, L_T , and average path length between a node and the array boundary, L_{mean} . He identified two extreme end-member cases, an 'explosion' structure where all nodes are connected to the boundary by the most direct path. Characteristic features of this structure are that the total path length is very large, but the mean path length from individual nodes to the boundary is small. The converse case of the spiral pattern, where the total path length is relatively small but the mean path length from individual nodes to the boundary is relatively long. The intermediate case is a branching or bifurcating structure. This structure achieves full connectivity of the nodes for a low total path length and mean path length. Rodriguez-Iturbe et al. [1992] and Rinaldo et al. [1992] have argued that river networks have a branching or bifurcating structure as this is the optimal configuration with respect to energy expenditure.

Stevens [1974] described the range of patterns, and the resulting topographic properties, that could be generated by connecting a set of nodes in a 2-D plane. The arrays used in the EVOLVER study consist of fully connected lattices with apertures varying as a continuum. However, it is possible to correlate the three geometrical regimes of the evolved fracture networks, as shown in Figure 10, onto the patterns of connectivity described by Stevens [1974] if only the largest of the fracture apertures are

considered. For example, the regime associated with homogenised row apertures can be correlated with the explosion structure, i.e. both are structures with short path lengths (for the relatively enlarged apertures) for individual nodes. The regime of heterogeneous anastomosing fracture apertures may be correlated with the branching or bifurcating structure, and is associated with a high degree of connectivity of relatively large aperture fractures, relatively low total path length and mean path length. The regime of the single preferentially enlarged array-spanning aperture may correspond to the spiral pattern where the total path length of relatively enlarged apertures is relatively small but the mean path length from individual nodes to the boundary is relatively long (depending on the tortuosity of the path).

Given constant a_0 and σ_{a0} , why do small aperture growth-rate exponents lead to the 'explosion' type development of increasingly homogeneous row apertures and larger aperture growth-rate exponents lead to the growth of complex branching aperture arrays or preferentially enlarged array-spanning paths as illustrated in Figure 2? The fracture arrays evolve as a result of competition between changes in the local and overall head and flow gradients and changes in the aperture distribution, and in each structural regime different components of the network control the evolution of the system as a whole.

At low aperture growth-rate exponents, e = 0.2 to 0.3 (and at low values of σ_{a0}), the macroscopic head distribution dominates the development of the arrays because the largest column-oriented apertures cannot grow fast enough to transfer significant flow between the row-oriented fractures. Head gradients are much larger along the row-oriented fractures than along the column oriented-fractures and flow is controlled by the smallest apertures in the parallel-configured row apertures. Row aperture homogenisation is achieved by the sequential enlargement of the smallest parallel-configured row apertures at each time step. Column apertures develop more slowly, due to local 'mismatches' in heads down the macroscopic head gradient between neighbouring rows. The evolved column apertures remain lognormally distributed due to their pseudo-random mode of growth (Figure 3).

At higher values of the aperture growth-rate exponent, e = 0.3 to 0.6 (and at higher values of σ_{a0}), relatively large column apertures can develop fast enough to enable significant heterogeneities in the local head and flow gradients to develop and compete with the macroscopic head gradient for the control of the development of the array. The development of a limited number of preferentially enlarged column apertures enables flow to by-pass the smallest apertures in the row-oriented fractures (rather than be concentrated through them) and leads to the development of complex anastomosing growth patterns like those seen in Figure 2 for runs 30, 27 and 32.

At large aperture growth-rate exponents (i.e. e = 0.7), the smallest aperture in an array-spanning path can develop fast enough to compete with larger apertures in the array away from the path and will control the overall development of the array. Under these conditions a preferentially enlarged array-spanning path develops. Once developed, flow is concentrated along the path and, like the low aperture growth-rate exponent regime, apertures in the array-spanning path are homogenised by sequential enlargement of the smallest aperture in the path at each time step. This interpretation of the formation of the preferentially enlarged array-spanning paths is consistent with the observation that at lower values of σ_{a0} the evolved paths are less tortuous (Figures 5 and 6).

5.3 Transmissivity of the Evolved Aperture Arrays

A class of percolation theory sometimes know as "critical path analysis" (CPA) [David, 1993] has been developed to describe the conductance of fully connected networks where the range of apertures is very wide [Ambegaokar, et. al., 1971; Berman et al., 1986; Charlaix et al., 1987; Feng et al., 1987; Stauffer and Aharony, 1994; Bernabe and Bruderer, 1998]. The following section discusses how well the transport properties of some of the aperture arrays generated by EVOLVER can be estimated using CPA.

A model to describe the conductive properties of fully connected heterogeneous networks was first proposed by Ambegaokar et al. [1971]. They suggested that in fully connected systems where the range of apertures is very broad the overall conductance of a network, S, is approximately equal to a critical conductance, s_c , defined by a minimum conductance of a subset of conductances which spans the network when arranged in descending order. This subset forms a backbone with exactly the percolation threshold concentration, p_c [Stauffer and Aharony, 1994]. For sufficiently broad distributions (i.e., conductance ratios greater than about 100), the conductance of the backbone is a good estimate of the overall conductance of the network. This can be illustrated by considering the structure of the backbone, and the structure of the network away from the backbone. The backbone will largely consist of fractures with conductances grater than s_c arranged in series-parallel orientations, these fractures will not limit the overall conductance of the network. The fractures away from the backbone will have conductances $s < s_c$, and isolated conductances $s > s_c$. The isolated fractures with conductances greater than the critical conductance will not effect the overall conductance of the network because they will be surrounded by low conductance fractures. The low conductance fractures will make a negligible contribution to the overall conductivity of the network as they will be effectively shorted out by the conducting backbone. Berman et al. [1986] tested this proposition by performing a series of simulations on resistor networks of varying size, using a range of initial distributions (uniform, gaussian, lognormal and cubic) and a range of distribution widths. On the basis of between 70 and 100 realisations for each set of initial conditions, they found good agreement between s_c and S, even for lognormal distributions where the half-width of the distribution was 10^8 .

The transport model of *Ambegaokar et al.* [1971] requires a random distribution of conductances. Consequently, the initial aperture arrays in our aperture growth model should exhibit the same behaviour as predicted by *Ambegaokar et al.* [1971] and *Berman et al.* [1986]. This can be tested if s_c is equated with the transmissivity of the critical fracture, T_{crit} , where $T_{crit} = a_c^3$, and a_c is the aperture of the critical fracture in the percolating backbone, and if S is equated with T_{eff} in Equation (15). Two methods can be used to find the critical aperture. Either, the apertures are ranked and added consecutively to an aperture map until a critical array-spanning path is obtained (the last fracture added corresponding to the critical aperture). $T_{crit(map)}$ can then be calculated. Or, because we are using a regular grid (two-dimensional square lattice) for which the bond percolation threshold is known ($p_c = 0.5$) [*Berman et al.*, 1986; *Stauffer and Aharony*, 1994], a_c can be approximated by the 50th percentile of the ranked aperture distribution and $T_{crit(50)}$ can be calculated. Table 1 gives values of T_{crit} (obtained for both methods) and of T_{eff} for the initial aperture distributions of six runs ($\sigma_{a0} = \log_{10} 0.3$ and $a_0 = \log_{10} 0$). Table 1 shows that, as the model predicts, there is a good one to one correspondence between T_{crit} (map) and T_{eff} and between T_{crit} (map) and mathematical aperture distributions.

As the apertures in the evolved arrays become more self-organised it may be expected that T_{crit} will no longer be a good measure of T_{eff} . This is illustrated in Figure 13, which shows changes in the T_{crit}/T_{eff} ratio with time for aperture growth-rate exponents in the range 0.2 to 0.7 ($\sigma_{a0} = \log_{10} 0.3$ and $a_0 = \log_{10} 0$). The error bars on the 0.7, 0.5 and 0.3 growth-rate exponent curves (1 S.D.) are based on ten runs at each condition. Runs at higher growth-rate exponents systematically depart from a T_{crit}/T_{eff} ratio of one, and comparison of Figures 7 and 13 shows that the T_{crit}/T_{eff} ratio increases rapidly at high aperture growth-rate exponents due to a large increase in T_{crit} . However, at low growth-rate exponents (e = 0.2 and 0.3) the T_{crit}/T_{eff} ratio remains approximately constant even though there are large increases in T_{eff} (Figure 7). T_{crit} appears to be a useful descriptor of T_{eff} in this range despite the evolved arrays being highly ordered, non-percolating, structures (Figure 2). This is because in these evolved arrays the row-oriented fracture apertures are homogenised and all row-oriented apertures approach the aperture of the critical fracture.

Table 1. Values of T_{crit} and T_{eff} for the initial aperture distributions of six runs ($\sigma_{a0} = \log_{10} 0.3$ and $a_0 = \log_{10} 0$). Values of $T_{crit(map)}$ were found using the map construction method and values of $T_{crit(50th)}$ were calculated from the 50th percentile of the ranked aperture distribution.

Run	$T_{crit(map)}$	$T_{crit(50th)}$	$T_{\it eff}$	$T_{crit(map)}$ / $T_{e\!f\!f}$	$T_{crit(50th)}$ / T_{eff}
98	0.588	0.820	0.768	0.766	1.068
99	1.099	0.985	1.023	1.074	0.963
100	0.659	0.899	0.945	0.697	0.951
101	1.106	0.985	0.988	1.119	0.997
102	1.052	1.071	1.129	0.932	0.948
103	1.218	1.080	1.229	0.991	0.879
104	1.067	1.027	0.980	1.089	1.048
105	0.823	0.893	0.917	0.897	0.974
106	1.106	1.049	1.033	1.070	1.015
107	0.879	0.904	0.869	1.012	1.041
mean	0.960	0.971	0.988	0.965	0.988
S.D.	0.212	0.088	0.129	0.142	0.057

Charlaix et al., [1987] and Bernabe and Bruderer, [1998] have extended CPA and percolation theory arguments to model the conductance of continuum percolation sub-networks away from p_c . Charlaix et al., [1987] modelled the permeability of a random array of fractures with widely varying apertures and placed upper and lower bounds on the permeability of sub-networks between p_c and p=1. Bernabe and Bruderer, [1998], who studied the effect of variance of pore size distribution on the transport properties of heterogeneous networks, modelled changes in a connectivity function and permeability as a function the maximum pore size in sub-networks in the range p=0 to 1. Due to spatial correlations in the evolved arrays there are systematic differences between values of T_{eff} and values of transmissivity predicted by CPA (Figure 13). Similarly, the transport behaviour of sub-networks in the evolved arrays is also expected to systematically depart from that predicted by Charlaix et al., [1987] and Bernabe and Bruderer, [1998]. However, this has not been investigated.

Figure 13. Variation in $T_{crit(map)}$ / T_{eff} as a function of time for aperture growth-rate exponents in the range 0.2 to 0.7 ($\sigma_{a0} = \log_{10} 0.3$ and $a_0 = \log_{10} 0$). Error bars on the 0.7, 0.5 and 0.3 aperture growth-rate exponent curves are based on ten runs at each condition.

One of the generic assumptions of the EVOLVER model (assumption C) was that the fractures consist of finite lengths over which the aperture is uniform. Based on this assumption, the velocity of flow through a fracture is given by the product of fracture conductivity and head gradient across the fracture (Equation 4), where the conductivity is a function of fracture aperture (Equation 10). All the runs that have been described previously were generated assuming plane fracture flow through individual fractures, i.e. flow rate was taken to be proportional to the cube of the aperture [Barker, 1993] (f was set to unity and g to 3 in Equation 10). This was thought to be reasonable given the uniform fracture aperture assumption. However, departures from the 'cubic law' may be envisaged if the aperture of individual fractures is not uniform [Silliman, 1989].

To assess the affects of relaxing the 'cubic law' condition, a limited number of runs were performed with values of g in the range 3 to 2. Figure 14 shows three evolved aperture arrays at time 100 ($\sigma_{a0} = \log_{10} 0.3$, $a_0 = \log_{10} 0$ and e = 0.6). Figures 14a, 14b and 14c were generated with g = 2, 2.5 and 3 respectively. Figure 12d shows T_{eff} as a function of time for five values of g between 3 and 2. Although the evolved structures do not look significantly different from those generated assuming the 'cubic law', it can be seen from Figures 14a to 14c that higher values of g tend to promote the development of preferentially enlarged, array-spanning, aperture paths, and that lower values of g tend to lead to more homogeneous enlargement of fracture apertures parallel to the head gradient. As expected, Figure 14d shows a decrease in T_{eff} at lower values of g, with T_{eff} for g = 2 at time 100 approximately two orders of magnitude less than the equivalent value for g = 3.

Figure 14. Illustration of the effects of relaxing the 'cubic law' condition. The figure shows three evolved aperture arrays at time 100 ($\sigma_{a0} = \log_{10} 0.3$, $a_0 = \log_{10} 0$ and e = 0.6), where Figures 14a, 14b and 14c were generated with g = 2, 2.5 and 3 respectively. Figure 14d shows T_{eff} as a function of time for five values of g between 2 and 3.

5.4 Limitations of the Model

The initial motivation for the study was to develop a model to help in the investigation of aquifer development, and, specifically, to investigate the development of enhanced fracture porosity in the Chalk. However, we see a number of limitations to the existing EVOLVER model when applying it to natural hydrogeological systems. This is due to some of the simplifying assumptions that were necessary when developing the generic model.

For example, it is assumed that the fracture network is fully connected. In addition to being physically implausible (i.e. matrix blocks floating between fracture surfaces), this assumption is geologically unreasonable. The connectivity of fractures and the range of typical primary apertures of fractures in shallow aquifers vary significantly with depth. Fracture connectivity and primary apertures are expected to increase towards the ground surface due to stress relief processes, and immediately below ground level fractures are expected to be essentially fully connected [*Bloomfield*, 1996], however, at depth the degree of fracture connectivity may be reduced. *Renshaw* [1996] has suggested that many natural fracture networks have spatial densities near the percolation threshold and that this may be due to the existence of self-limiting mechanisms in the formation of fracture networks. The architecture of the primary fracture networks may be expected to influence the subsequent development of fracture arrays.

Another potentially unrepresentative feature of the work described in this paper is the inability of the model to account for concomitant reduction in the apertures of some of the fractures. If fracture closure occurs in association with aperture growth, for example by clogging with mechanically derived particles from other parts of the fracture array, or by re-precipitation, then fundamentally different aperture arrays may develop. *Rege and Fogler* [1989] modelled permeability variation in an idealised porous network undergoing both dissolution and precipitation. The permeability of the medium was found to fluctuate widely with flow rate, and no systematic relationships could be identified between these variables. Even if there is no fracture closure mechanism in operation, aperture growth-rates may vary spatially under natural hydrogeological conditions.

Perhaps more importantly, the EVOLVER model assumes that the boundary conditions are fixed throughout the development of the array. For example, the EVOLVER model has been used in a constant flux mode. However, in natural systems the flux may change over a range of time scales (from days to thousands of years). In the model any changes in the magnitude of the flux may affect the local head and flow distributions in the aperture array and hence the evolved structure of the array. Because the evolved structures are amplified from the initial boundary conditions, any changes in flux, particularly in the early stages of array development, could lead to significant changes in the overall structure of the evolved arrays. The sensitivity of the EVOLVER model to a relaxation of any of the initial boundary conditions during a run, including changes in flux, has not yet been assessed.

To date EVOLVER has not been validated. Because a generic approach has been adopted, EVOLVER is not readily amenable to validation in any general sense, but two possible approaches to the problem of model validation can be envisaged. First, if a variety of measures of the spatial structures resulting from the model can be developed then these measures could, at least in principle, be compared when applied to the evolved structures and with measures taken from real-world data (e.g. fracture patterns). If possible, it would be useful to simultaneously make comparison with the measures for other models of structures (e.g. fractal models). The most effective combination of measures would need to be investigated. However, a more appropriate form of validation is in terms of the ability of the model to reproduce flow or transport data (especially pumping-test and tracer results). The EVOLVER model could be tested in (at least) two quite different methods, both of which require calibration against data. Firstly, evolved structures could be taken as starting points ('templates') which are refined by a method such as simulated annealing. Alternatively, if we recognise the evolved structures as resulting from a rather small number of control parameters

(including time), we can calibrate the model against data using almost any standard minimisation procedure (e.g. simplex or conjugate gradient) which can adjust those parameters. This form of validation is likely to be computer intensive. A significant part of work on the development of validation methodologies for EVOLVER would use synthetic data from relatively simple structures so that validation and sensitivity analysis can be precise.

5.4.1 Limitations of EVOLVER with respect to modelling Chalk aguifer development

In the Chalk it is not unreasonable to infer that groundwater recharge near the top of the aquifer is slightly more chemically aggressive than groundwaters at depth, particularly near Palaeogene cover. Therefore, if the entire thickness of the Chalk aquifer were to be modelled a more realistic starting condition for EVOLVER would consist of a layered model with aperture growth rate exponents decrease with depth. In addition, the model assumes that the fractures are fully saturated, i.e. that there is no water table or capillary fringe in the model. To introduce a water table into the model would require the imposition a remote boundary condition with the notional pinning of a water table at a remote discharge point. Movement of a water table through the array would need a re-scaling of the flux proportional to the reduced area of saturation to maintain the constant flux boundary condition. At the interfluve scale it may be reasonable to expect the water table to fall if fracture apertures become enlarged. There are many observations that water tables in the Chalk are commonly associated with horizons of pronounced fracturing *Foster and Milton* [1974] and *Price et al.* [1977, 1982, 1993]. Any revised model involving a water table should account for these observations and would need to incorporate appropriate remote boundary conditions.

The present EVOLVER model is dimensionless. However, if it is to be used to model field data (initial and/or evolved aperture distributions), then it will be necessary to scale parameters in the model. These would include array dimensions, fracture aperture and growth-rate, groundwater flux and heads, and time. It has been noted (Section 2) that the separation of nodes in the fracture aperture maps, e.g. Figure 2, has been fixed at an arbitrary length scale, so that the evolved apertures do not overlap in the graphical presentation. The results of aquifer scale models could not be visualised without rescaling some parameters.

5.5 Requirements for a Quantitative Description of Dynamic Systems such as EVOLVER

In this study the descriptions of the evolved arrays have been restricted to qualitative descriptions and simple statistical measures, however there is a need to develop a quantitative description of the system. Given that the model is formulated as an initial value problem, it should be possible to predict the form of the evolved structures on the basis of the initial boundary conditions (no additional information should be necessary). We are aware that related studies have been performed in a wide variety of fields (e.g. geometrical percolation, electrical networks, topology, self-organisation, and non-linear systems), and these could be used as possible starting points for the development of a quantitative description of the dynamic system. However, we are also aware of the many problems related to predicting the behaviour of complex systems exhibiting emergent behaviour [Holland, 1998].

Any theoretical model should identify characteristic parameters of the evolving pore structures and should be capable of predicting important features of the behaviour of the system. For example, characteristic parameters are expected to be related to existing topological or percolation parameters and may include connectivity, a dynamic critical threshold, characteristic dynamic cluster properties and scaling constants. If it is possible to identify characteristic parameters they could be used to direct the measurement or sampling of natural systems. Important features of the system that any theoretical model should be capable of predicting include the formation of dynamically stable self-organised structures, and geometrical phase changes in the evolved structure as a function of changes in initial boundary conditions.

In addition, any theoretical model should also be capable of specifically predicting the growth of the array-spanning structures. Percolation theory may provide a suitable starting point for description of the evolution of structures near this phase change (although it would not provide an appropriate description of the evolution of other arrays away from this phase boundary) [Stauffer and Aharony, 1994]. Unlike classical percolation problems [Sahimi et al., 1990], the EVOLVER model is formulated as a fully connected array (p=1), with apertures continuously distributed about a mean, and where the array-spanning paths develop as the result of a dynamic feedback process. We are unaware of any existing percolation theory that describes the geometry of fully connected systems undergoing 'dynamic' continuum percolation, but any extension of percolation theory may enable recognition of universal scaling relationships in the growth of the array-spanning paths.

6. SUMMARY

A simple model, EVOLVER, based on a limited number of assumptions and based on simple growth laws applied to idealised pore (fracture aperture) structures with simple initial aperture distributions, has been used to investigate patterns of porosity development in response to flow. The approach adopted is similar to that of statistical mechanical studies of simple systems, where the evolved structures depend on the initial values. A feedback process used by EVOLVER to generate porosity evolution gives rise to a range of self-organised or emergent structures. The development of self-organised structures is a characteristic feature of many geological processes that involve feedback between rock properties and flow and/or transport. For example, *Ortoleva et al.*, [1995] have shown how reaction-transport models can be used to explain self-organised structures in sedimentary basins over a wide range of scales (megascopic basin-wide phenomena to mesoscopic phenomena at the mm to m scales). However, unlike the models described by *Ortoleva et al.*, [1995], transport is not implicit in the EVOLVER model. EVOLVER does not track 'packets' of water and there are no reaction gradients across the modelled arrays. EVOLVER demonstrates that it is possible to generate self-organised pore structures in geological materials solely as a result of flow, independent of chemical concentration and/or reaction gradients.

A characteristic feature of simple systems with variable boundary conditions is the potential for phase changes. Using EVOLVER it has been shown that given a spatially uncorrelated initial aperture distribution even small changes in the initial model values can lead to large qualitative changes in the structure of the evolved arrays. Because of the diversity of the evolved structures it is difficult to identify appropriate geometrical parameters to characterise the arrays and to define the observed geometrical phase changes. However, using only a simple statistical measure, the standard deviation of fracture apertures oriented parallel to the direction of bulk flux, it has been possible to characterise regimes of evolved structures corresponding to a specific range of initial values.

The evolved structures are highly sensitive to initial boundary conditions, and for the range of initial boundary conditions considered, aperture distributions appear to become both statistically and geometrically stable. The diverse structures that develop range from the relatively uniform development of row-parallel apertures to the development of preferentially enlarged single array-spanning paths, where the tortuosity of the preferentially enlarged array-spanning paths is a function of the breadth of the initial aperture distribution.

Further investigation requires the development of a quantitative description of the system that is capable of predicting the formation of dynamically stable self-organised structures and geometrical phase changes in the evolved structure as a function of changes in initial boundary conditions. It should also include the identification of appropriate parameters to characterise the evolving arrays. However, the task is not trivial as there are many problems related to predicting the behaviour of complex systems exhibiting emergent behaviour.

7. FUTURE WORK

A proposal for additional work related to EVOLVER was submitted to the NERC Micro-to Macro Thematic Programme and was awarded funding in March 1999. The project will last for two years and will start early in the financial year 1999/2000. The following section outlines the work included in the Micro-to-Macro project.

There are six strands within the project:

- Review of the processes of porosity development and their dependence on hydrodynamic flow, and of generic hydrogeological scenarios (boundary conditions).
- The development of a theoretical framework to describe the dynamic behaviour of evolving porous media.
- Code development.
- Model validation.
- Investigation of scaling and self-organisation phenomena in simple systems.
- Case studies

7.1 Review

The aim of the initial phase of the project will be to identify the constraints on the model. Firstly, we will review previous studies of porosity development processes and identify the constitutive forms of growth laws for each process. Specific attention will be paid to porosity development processes and growth laws associated with carbonate dissolution. The BGS/UCL scoping study (described in Sections 1 to 6 of this report) used a very simple aperture growth law. The appropriateness of this law will be assessed in the light of the process-specific growth laws, and new generic growth laws will be formulated and used in the study if necessary. In addition, we will review work on effective porosity growth laws. Secondly, we will review the scenarios (boundary conditions) that the code will be required to model. These will include reviews of characteristics hydraulic boundary conditions and initial pore geometries and aperture distributions. It will also include an assessment of the most appropriate network co-ordination number to use in the model (an orthogonal network was used in the scoping study, however, other networks such as triangular or hexagonal networks, and partially saturated networks may be more appropriate). The results of this review will be used as a basis for defining the range of initial boundary conditions that can be investigated using the generic model.

7.2 Theoretical Development

We are aware that related studies have been performed in a wide variety of fields (e.g. geometrical percolation, electrical networks, topology, self-organisation, non-linear systems and chaos). As an initial activity, we will review all relevant literature and will seek, where appropriate, collaboration with researchers currently active in these fields. In particular we would be interested in different methods of characterising networks and network evolution. Wherever possible we would adapt the methods and results to be applicable to the present study (for example electrical resistivity is equivalent to the reciprocal of permeability). Network theory has been used to describe flow through systems of connected pore structures, and percolation theory has been developed to describe the scaling behaviour of structures near their connectivity threshold. Results from the scoping study suggest that the dynamic growth of highly connected pore networks (well above the percolation threshold) exhibits percolation-like behaviour. Given that the problem is conceptualised as a

deterministic initial value problem, we hope to develop a theoretical approach to predict the spatial and scaling properties of evolving pore and flow distributions as described previously in Section 5.5. Predictions based on theoretical developments will be tested using the model code.

7.3 Code Development

The existing code, EVOLVER, used in the scoping study will be the starting point for code development. The generic code will be flexible and will include 'through flow', flow to a point and periodic boundary conditions. A library of standard initial distribution functions (e.g. normal, exponential, gamma) will be available in addition to user defined distributions. Consideration will be given to (i) the appropriateness of such distributions in relation to rock morphology given the implicit constraints on the distributions (based on the information theory approach) and (ii) the potential for developing more appropriate distributions from those same considerations. There will be <u>full flexibility</u> to the form of the growth law that can be studied. User defined growth laws will be accommodated as well as default growth laws expressed as n'th order polynomial functions of a range of parameters, including flux and aperture.

EVOLVER has been used to model the development of porosity in an orthogonal 2-D array. The code currently uses a square mesh template, and the code will be revised so that the co-ordination number of the nodes in the array is variable. We need to investigate the dependence of the evolved structures on that template. We will compare results obtained using meshes based both on crystallographic and random-packing geometries. (In the latter case we will probably need to use bandwith reduction methods to ensure efficient solution of the linear equations.) A specific activity will be to investigate the influence of grid size (e.g. 20×20, 100×100) on the results (see Section 7.5.b. below) and hence the selection of appropriate grid sizes. The code will be revised so that the modelled array can be either 2- or 3-D. The extension to a 3-D grid poses no problem in terms of the mathematical formulation, which was deliberately made geometry independent, but there will be a significant increase in the computational demands of solving the flow equations. Several methods of solving the equations have been tried and a relatively simple LSOR technique has proved robust and competitive with other methods given the simple grid geometry adopted so far. Amongst other methods that have been tried is a sparse-equation method. When that latter type of method is employed any connectivity or dimension can be handled. It is therefore envisaged that a sparse subroutine method will be used to obtain the flexibility desired. The choice of routine is a specific task that will be addressed. It will depend on the computing platform and need to take advantage of the particular form of the matrix, such as it being positive definite. A conjugate-gradient method appears, in principal, to be favoured. It is recognised, however, that since a good estimate of the solution is always available, except initially, an iterative solution may prove to be the most effective, especially if a parallel machine is used. Going from an N×N square grid to an N×N×N cubic grid, for example, would increase computing time, even for a conjugate gradient method, by somewhat more than a factor of 2N and dynamic memory requirements by a similar factor. This is substantial, so one of the NERC supercomputers will be used for selected modelling runs.

No spatial correlation is built into the initial porosity distributions in the EVOLVER code. This feature will be retained in the revised code because we wish to study the processes of self-organisation during porosity evolution. The revised code will be flexible with respect to porosity growth laws and will include the option for rules about growth of neighbouring structures (cellular automata). In addition to the above developments, other changes will be made to make the model more flexible for use in the case studies (described in Section 7.5). The code will be revised so that the degree of pore connectivity can be increased (porosity or fracture nucleation) or decreased (pore or fracture clogging or cementation) during a model run. In addition, it will be made possible to (i) modify boundary conditions during a run, i.e. systematically increase flux or head as the model evolves and (ii) apply different porosity growth laws over different parts of the array. EVOLVER is a stochastic model but the revised code will enable the initial porosity array to be specified explicitly as

well as stochastically. The code will be compiled in Fortran 90 and will run on PCs (small arrays only) and workstations (large arrays and 3-D arrays). As mentioned above NERC supercomputer time is being requested for the study of large arrays and for multiple realisations. The existing EVOLVER code includes a number of sub-routines with limited post-processing capabilities that provide quantitative measures of network heterogeneity. We propose to develop those routines into a separate software suite that would produce further 'measures' (e.g. those based on percolation theory). We will further develop our ability to visualise the networks and will be purchasing appropriate software; we aim, for example, to provide stereo pairs for visualisation of 3-D arrays.

7.4 Model Validation

As has already been noted, the proposed model of porosity development will be generic and therefore not amenable to validation in any general sense. It is not intended that any significant validation be carried out during this relatively short project but the resulting code will be made available for validation by other researchers against their data. What will be required, however, is a proven methodology for carrying out such validation. Therefore one task in our programme of work will be to explore several approaches to validation to provide guidelines and, if possible, software aids. Two general approaches have already been outlined in Section 5.4.

7.5 Scaling Phenomena in Simple Systems

The revised code will be used in its most general form to investigate scaling phenomena related to porosity development in simple systems and to test theoretical developments (Section 7.2). Five areas have been identified for particular investigation:-

- (a) the nature of porosity self-organisation and scaling characteristics as a function of the boundary conditions (i.e. a more quantitative and more fully parameterised approach than has been afforded, so far, by visualisation)
- (b) the existence, or otherwise, of a representative elementary volume during network evolution under a wide range of boundary conditions. Findings will be compared with the results of a study of scaling relationships, probably using upscaling methods.
- (c) using synthetic pumping test databased on the generated networks, the evolution of flow dimension [Barker, 1988] and scale-dependent dispersivity will be investigated. There are difficulties in interpreting non-integer flow dimensions and they may be scale-dependent. Therefore, the generated networks offer an ideal opportunity to investigate flow dimensions systematically.
- (d) the effect of 'decorated' or fractal initial networks (each initial pore consists of a sub-set of pores) on the scaling behaviour of the evolved structures, and
- (e) the sensitivity of the evolved arrays to small changes in initial boundary conditions (chaotic systems).

Since the project is based on a modest budget, only a limited number of specific investigations have been identified. However, we envisage that the work will spawn further research ideas that could be developed by other partners within and beyond the Programme.

7.6 Case Studies

Complementary porosity growth problems or scenarios will be modelled as case studies to demonstrate the utility of the EVOLVER model. These will use versions of the revised code where the boundary conditions may vary with time, the initial array is pre-conditioned, and specific,

functional porosity growth laws will be investigated. Under these circumstances the model will be qualitatively different to the simple systems studied in section 4. Two specific problems that will be studied are (a.) the development of fracture aperture distributions in carbonate aquifers at the local to sub-regional scale (including an assessment of differences in evolved fracture arrays due to dissolution and mechanical abrasion processes) and (b) the development of porosity in relatively friable sandstones near pumped boreholes ('flow to a point' problem). The remaining topic(s) will include the generation of synthetic stochastic pore or fracture distributions for use in other models/studies to be suggested by other groups in the Programme.

REFERENCES

- Acuna J A and Yortsos Y C 1995. Application of fractal geometry to the study of networks of fractures and their pressure transient. *Water Resour. Res.*, 31(3), 527-540
- Andersson J and B Dverstrop1987. Conditional simulations of fluid flow in three-dimensional networks of discrete fractures, *Water Resour. Res.*, 23(10), 1876-1886
- Ambegaokar V, Halperin B I, and Langer J S 1971. Hopping conductivity in disordered systems. *Phys. Rev. B.*, *4*, 2612-2620
- Atkinson B K 1984. Subcritical crack growth in geological materials. J. Geophys. Res., 89, 4077-4114
- Bak P, Tang C and Wiesenfeld K 1988. Self-organised criticality. Physical Review A, 38, 364-374
- Bak P 1996. How nature works The science of self-organised criticality, Copernicus
- Barker J A. A generalised radial flow model for pumping tests in fractured rock. *Water Resour. Res.*, 24(10), 1796-1804.
- Barker J A 1993. Modelling groundwater flow and transport in the Chalk, in *The Hydrogeology of the Chalk of North-West Europe*, edited by R A Downing, M Price and G P Jones, pp. 60-66, Clarendon Press, Oxford
- Bloomfield J P 1996. Characterisation of hydrogeologically significant fracture distributions in the Chalk: and example from the Upper Chalk of southern England. *J. Hydrol.*, *184*, 355-379
- Berkowitz B 1995. Analysis of fracture network connectivity using percolation theory. *Math. Geol.*, 27, 467-483
- Berkowitz B and Balberg I 1993. Percolation theory and its application to groundwater hydrology. *Water Resour. Res.*, 29(4), 775-794
- Berman D, Orr B G, Jaeger H M and Goldman A M 1986. Conductances of filled two-dimensional networks. *Phys. Rev. B.*, *33*, 4301-4302
- Bernabe Y and Bruderer C 1998. Effect of the variation of pore size distribution on the transport properties of heterogeneous networks. *J. Geophys. Res.*, 103, 513-525
- Brown S R and Scholz C H 1985a. Closure of random elastic surfaces in contact. *J. Geophys. Res.*, 90, 5531-5545, 1985a.
- Brown S R and Scholz C H 1985b. Broad bandwidth study of the topography of natural rock surfaces. *J. Geophys. Res.*, 90, 12,575-12,582
- Cacas M C, Ledoux E, Marsily G de, Tillie B, Barbreau A, Durand E, Feuga B and Peaudecerf P 1990a. Modelling fracture flow with a stochastic discrete fracture network: Calibration and validation, 1, The flow model. *Water Resour. Res.*, 26(3), 479-489
- Cacas M C, Ledoux E, Marsily G de, Barbreau A, Calmels P, Gaillard B and Margritta R 1990b. Modelling fracture flow with a stochastic discrete fracture network: Calibration and validation, 2, The transport model. *Water Resour. Res.*, 26(3), 491-500

- Charlaix, E, Guyon E and Roux S 1987. Permeability of a random array of fractures of widely varying apertures. *Transp. Porous Media*, 2, 31-43
- Daccord G 1987. Chemical dissolution of a porous medium by a reactive fluid, *Phys. Rev. Lets.*, 58, 479-482
- Daccord G and Lenormand R 1987. Fractal patterns from chemical dissolution, *Nature*, 325, 41-43
- Daccord G, Touboul E and Lenormand R 1989. Carbonate acidizing: toward a quantitative model of the wormholing phenomenon, *SPE Prod. Engn.*, *3*, 63-68
- David C 1993. Geometry of flow paths for fluid transport in rocks. J. Geophys. Res., 98, 12267-12278
- Dienes J K 1982. Permeability, percolation and statistical crack mechanics, in *Issues in Rock Mechanics*, edited by R. E. Goodman and F. E. Heuze, pp. 86-94. American Institute of Mining, Metallurgy and Petroleum Engineers, New York
- Dijk P and B Berkowitz 1998. Precipitation and dissolution of reactive solutes in fractures. *Water Resour. Res.*, 34(3), 457-470
- Downing R A, Price M and Jones G P 1993. *The hydrogeology of the Chalk of North-West Europe*, p. 300, OUP, Oxford
- Dreybrodt W 1990. The role of dissolution kinetics in the development of karst aquifers in limestone: A model simulation of karst evolution. *J. Geol.*, 98, 639-655
- Dreybrodt W 1996. Principles of early development of karst conduits under natural and man-made conditions revealed by mathematical analysis of numerical models. *Water Resour. Res.*, 32(9), 2923-2935
- Dullien F A L 1979. Porous Media: Fluid Transport and Pore Structure, Academic, San Diego, California
- Dverstorp B, Anderson J and Nordqvist W 1992. Discrete fracture network interpretation of field tracer migration in sparsely fractured networks, *Water Resour. Res.*, 28(9), 2327-2343
- Edmunds W M, Darling W G, Kinniburgh D G, Dever L and Vachier P 1992. *Chalk groundwater in England and France: hydrogeochemistry and water quality*, British Geological Survey Research Report SD/92/2, British Geological Survey, Nottingham
- Feng S, Halperin B I, and Sen P N 1987. Transport properties of continuum systems near the percolation threshold, *Phys. Rev. B.*, 25, 197-214
- Foster, S D D and Milton V A 1974. The permeability and storage of an unconfined chalk aquifer. *Hydrol. Sci. Bull.*, 19, 485-500
- Groves C G and Howard A D 1994a. Minimum hydrochemical conditions allowing limestone cave development. *Water Resour. Res.*, 30(3), 607-615
- Groves C G and Howard A D 1994b. Early development of karst systems. 1. Preferential flow path enlargement under laminar flow. *Water Resour. Res.*, 30(10), 2837-2846
- Gueguen Y, David C and Darot M 1986. Models and time constants for permeability evolution. *Geophys. Res. Letts.*, 13, 460-463

- Hakami E and Barton N 1990. Aperture measurements and flow experiments using transparent replicas of rock joints, in *Rock Joints*, edited by N., Barton and O., Stephansson, Balkema, Rotterdam, 1990. pp.383-390
- Hoefner M L and Fogler H S 1986. Reaction rate vs. transport limited dissolution during carbonate acidizing: application of network model, *SPE 15573*, New Orleans, LA
- Hoefner M L and Fogler H S 1988. Pore evolution and channel formation during flow and reaction in porous media, *A.I.Ch.E. J.*, 34, 45-54
- Holland J H 1998. Emergence. From chaos to order, OUP
- Howard A D and Groves C G 1995. Early development of karst systems. 2. Turbulent flow, *Water Resour. Res.*, 31(1),19-26
- Lloyd J W 1993. The United Kingdom, in *The Hydrogeology of the Chalk of North-West Europe*, edited by Downing R A, Price M and Jones G P, OUP, Oxford, pp. 220-249
- Long J C S, Karasaki K, Davey A, Peterson J, Landsfeld M, Kemeny J and Martel S 1991. An inverse approach to the construction of fracture hydrology models conditioned by geophysical data. *Int. J. Rock Mech. Min. Sci. Geomech. Abstr.*, 28, 121
- Margolin G, Berkowitz B and Scher H 1998. Structure flow, and generalized scaling in fracture networks. *Water Resour. Res.*, *34*(9), 2103-2121
- Moreno L, Tsang Y W, Tsang C F, Hale F V and Neretnieks I 1988. Flow and tracer transport in a single fracture: A stochastic model and its relation to some field observations. *Water Resour. Res.*, 24(12), 2033-2048
- Nordqvist A W, Tsang Y W, Tsang C F, Dverstrorp B and Andersson J A 1992. A variable aperture fracture network model for flow and transport in fractured rocks. *Water Resour. Res.*, 28(6), 1703-1713
- Nordqvist A W, Tsang Y W, Tsang C F, Dverstrorp B and Andersson J A 1996. Effects of high variance of fracture transmissivity on transport and sorption at different scales in a discrete model for fractured rocks, *J. Contam. Hydrol.*, 22, 39-66
- Ortoleva P, Al-Shaieb Z and Puckette J 1995. Genesis and dynamics of basin compartments and seals. *Am. J. Sci.*, 295, 345-427
- Palmer A N 1975. The origin of maze caves, Natl. Speleol. Soc., 37, 56-76
- Palmer A N 1991. The origin and morphology of limestone caves, Geol. Soc. Am. Bull., 103, 1-21
- Price M 1987. Fluid flow in the Chalk of England, Geol. Soc. Spec. Publ., 34, 141-156
- Price M, Downing R A and Edmunds W M 1993. The Chalk as an Aquifer, in *The Hydrogeology of the Chalk of North-West Europe*, edited by Downing R A, Price M and Jones G P, pp. 35-58, Clarendon Press, Oxford
- Rege S D and Fogler H S 1989. Competition among flow, dissolution, and precipitation in porous media, *A.I.Ch.E. J.*, *35*, 1177-1185, 1989.

- Renshaw C E 1996. Influence of subcritical fracture growth on the connectivity of fracture networks. *Water Resour. Res.*, 32(6), 1519-1530
- Rinaldo A, Rodrigues-Iturbe I, Rigon R, Bras R L, Ijjasz-Vasquez E and Marani A 1992. Minimum energy and fractal structures of drainage networks, *Water Resour. Res.*, 28(9), 2183-2195
- Roberts J N and Schwartz L M 1985. Grain consolidation and electrical conductivity in porous media, *Phys. Rev. B.*, *31*, 5990-5997
- Rodrigues-Iturbe I, Rinaldo A, Rigon R, Bras R L, Marani A and Ijjasz-Vasquez E 1992. Energy dissipation, runoff production, and the three-dimensional structure of river basins, *Water Resour*. *Res.*, 28(4), 1095-1103
- Sahimi M 1994. Applications of percolation theory, Taylor & Francis, London
- Sahimi M 1995. Flow and Transport in Porous Media and Fractured Rock, VCH, Weinhem
- Sahimi M, Gavalas G R and Tsotsis T T 1990. Statistical and continuum models of fluid-solid reactions in porous media, *Chem. Eng. Sci.*, 45, 1443-1503
- Siemers J and Dreybrodt W 1998. Early development of karst aquifers on percolation networks of fractures in limestones, *Water Resour. Res.*, 34(4), 409-420
- Silliman S E 1990. The influence of grid discretization on the percolation probability within discrete random fields, *J. Hydrology*, *113*, 177-191
- Silliman S E and Wright A L 1988. Stochastic analysis of paths of high hydraulic conductivity in porous media, *Water Resour. Res.*, 24(11), 1901-1910
- Smith L and Schwartz F W 1984. , An analysis of the influence of fracture geometry on mass transport in fractured media. *Water Resour. Res.*, 20(9), 1241-1252
- Stauffer D and Aharony A 1994. *Introduction to percolation theory*, (revised second edition), Taylor & Francis, London
- Stevens P S 1974. Patterns in Nature, Little, Brown, Boston, Mass
- Tsang, C-F 1993. Tracer transport in fracture systems, in *Flow and Contaminant Transport in Fractured Rock*, edited by Bear J, Tsang C-F and Marsily G de 1993. Academic Press, San Diego, pp. 237-266
- Tsang Y W 1984. The effect of tortuosity on fluid flow through a single fracture. *Water Resour. Res.*, 20(9), 1209-1215
- Tsang Y W and Tsang C-F 1987. Channel model of flow through fractured media. *Water Resour. Res.*, 23(3), 467-479
- Tsang Y W and Tsang C-F 1989. Flow channelling in a single fracture as a two-dimensional strongly heterogeneous permeable medium. *Water Resour. Res.*, 25(9), 2076-2080
- Tsang Y W and Witherspoon P A 1981. Hydromechanical behaviour of a deformable rock fracture subject to normal stress, *J. Geophys. Res.*, 86, 9287-9298

- Tsang Y W, Tsang C-F, Neretnieks I and Moreno L 1988. Flow and tracer transport in fractured media: A variable aperture channel model and its properties. *Water Resour. Res.*, 24(12), 2049-2060
- Walsh J B 1981. Effect of pore pressure and confining pressure on fracture permeability. *Int. Jour. Rock Mech. Min. Sci. Geomech. Abstr*, 18, 429-435
- Weyl P K 1958. Solution kinetics of calcite, J. Geol., 66, 163-176
- White W B 1977. Role of solution kinetics in the development of karst aquifers, *Mem. Int. Assoc. Hydrogeol.*, 12, 503-517
- Wong P-Z, Howard J and Lin J-S 1986. Surface roughening and the fractal nature of rocks. *Phys. Rev. Lett.*, *57*, 637-640
- Wong P-Z, Kiplik J and Tomanic J P 1984. Conductivity and permeability of rocks, *Phys. Rev. B.*, 30, 6606-6614
- Younger P L 1989. Devensian periglacial influences on the development of spatially variable permeability in the Chalk of southeast England. *Q. J. Eng. Geol.*, 22, 343-354

NOTATION

```
a_i aperture of fracture i.
```

 $\mathbf{a} = \{a_1, ..., a_N\}$ set of all apertures.

 $\mathbf{a_0} = \{a_{10}, ..., a_{N0}\}$ set of initial apertures.

A function formally characterising the dependence of apertures on time and model parameters.

 a_0 mean fracture aperture of the initial fracture aperture distribution.

 a_c aperture of the critical fracture.

 b_m parameter in equation (9).

 c_m parameter in equation (9).

 d_m parameter in equation (9).

 e_m parameter in equation (9), the aperture growth-rate exponent.

 f_m parameter in equation (10).

 g_m parameter in equation (10).

G function describing the rate of growth of a fracture.

 h_n head at node n.

H head at the upstream nodes \aleph_{μ} .

 ΔH head difference across the array parallel to the direction of bulk flux.

i fracture i.

K conductivity function.

 L_i length of fracture i.

 L_T total path length in an array of connected nodes.

 L_{mean} average path length between a node and an array boundary.

 $\mathbf{L} = \{L_1, ..., L_N\}$ set of fracture lengths.

N the number of fractures.

 \aleph_d the set of downstream (fixed-head) nodes.

 \aleph_u the set of upstream (fixed-head) nodes.

 \mathbf{p}^{K} a set of parameters characterising the relationship between aperture and conductivity.

 \mathbf{p}^G a set of parameters characterising the aperture change with time.

 \mathbf{p}^V a set of parameters characterising the volumetric flow rate.

p bond probability in (percolating) networks.

 p_c percolation threshold.

Q bulk flux across the fracture array.

S network conductance.

 S_c conductance of the critical component of a network

t time

 T_{eff} effective transmissivity of the fracture array.

 T_{crit} transmissivity of the critical fracture in an array.

 v_i the magnitude of the volumetric flow rate in fracture i ($v_i = |v_{jk}^i|$).

 v_{ik}^{i} the volumetric flow rate from node j to node k through fracture i.

V function formally describing the relationship of flux to head gradient.

tortuosity $(L_e/L)^2$, where L_e is the effective path length and L is the direct path length [Dullien, 1979].

 σ_{a0} standard deviation of the initial fracture aperture distribution.

 σ_{row} standard deviation of fracture apertures orientated parallel to the direction of bulk flux.